Drug-Encapsulating EGF-Sensitive Liposomes for EGF-Overexpressing Cancer Therapies

by

Albert Wong

Honors B.S. Biology
The University of Texas at Arlington, 2005

Submitted to the Harvard-MIT Division of Health Sciences and Technology in Partial Fulfillment of the Requirements for the Degree of

Master of Health Sciences and Technology

at the

Massachusetts Institute of Technology

May 2009

Signature of Author: _____
Division of Health Sciences & Technology
April 29, 2009

Mathematical models reviewed: _____
Klavs F. Jensen
Department Head and Warren K. Lewis Professor of Chemical Engineering
Professor of Materials Science and Engineering

Certified: _____
Robert S. Langer
Institute Professor

Accepted by: _____
Ram Sasisekharan
Edward Hood Taplin Professor of HST and Biological Engineering
Director, Harvard-MIT Division of Health Sciences & Technology

Drug-Encapsulating EGF-Sensitive Liposomes for EGF-Overexpressing Cancer Therapies

by

Albert Wong

Submitted to the Harvard-MIT Division of Health Sciences and Technology
on April 29, 2009 in Partial Fulfillment of the Requirements
for the Degree of Master of Health Sciences and Technology

Abstract

'Smart' targeted drug carriers have long been sought after in the treatment of epidermal growth factor (EGF)-overexpressing cancers due to the potential advantages, relative to current clinical therapies (generally limited to surgery, radiation therapy, traditional chemotherapy, and EGF receptor inhibitors (EGFRIs)), of using such 'smart' targeted drug delivery systems. However, progress toward this goal has been challenged by the difficulty of creating a drug carrier that can autonomously detect and respond to tumor cells in the body.

'Smart' micron-size drug-encapsulating epidermal growth factor (EGF)-sensitive liposomes for EGF-overexpressing cancer therapies have been developed and studied. These drug-encapsulating liposomes remain inert until they are exposed to an abnormal concentration of EGF. As a drug delivery system, these drug-encapsulating liposomes could release pharmaceutical agents specifically in the immediate neighborhood of tumors overexpressing EGF, thereby maximizing the effective amount of drug received by the tumor while minimizing the effective systemic toxicity of the drug.

Additionally, quantitative mathematical models were developed to characterize multiple critical rate processes (including drug leakage from drug-encapsulating liposomes and distribution of (drug-encapsulating) liposomes in blood vessels) associated

with (drug-encapsulating) liposomes in general. These quantitative mathematical models provide a low-cost and rapid method for screening novel drug-encapsulating liposome compositions, configurations, and synthetic methods to identify liposome compositions, configurations, and synthetic methods that would deliver optimal performance.

The results provide a stepping stone toward the development of EGF-sensitive liposomes for clinical use. More generally, they also present implications for future development of other targeted drug delivery vehicles.

TABLE OF CONTENTS

LIST OF ILLUSTRATIONS

Chapter 1

Introduction

The human body is fundamentally dependent on the process of mitosis to renew itself and repair damage. Although *in vivo* cell replication is typically a closely monitored and regulated process, the regulatory checkpoints are not infallible. Inevitably, given sufficient time, a few cells with harmful genetic mutations may evade apoptosis and go on to replicate. Certain mutations may lead to subsequent uncontrolled cell replication and further harmful genetic mutations, which, if not detected and stopped by the immune system, may lead to cancer [1].

Epidermal growth factor (EGF)-overexpressing cancers (i.e., cancers, often advanced cancers, that produce abnormal amounts of EGF), along with other types of cancers, have collectively drawn enormous treatment expenses [1],[2],[3]; for example, the anticancer therapy market in the seven major pharmaceutical markets alone was valued at ~$24 billion in 2006 [4]. As overall life expectancies increase, the net incidence of cancers and the resulting treatment expenses will only continue to rise. Hence, research toward better cancer therapies is of critical importance.

Currently, conventional treatments are usually limited to surgery, radiation therapy, and generalized chemotherapy. Radiation therapy and generalized chemotherapy may result in significant side effects, including an increased risk of new tumor formation. Surgery, when feasible, is attendant with the risk of various surgical complications. Worse, combinations of treatments, usually radiation therapy and generalized chemotherapy, and recurring treatments, such as recurring radiation therapy, are often necessary, typically resulting in additional side effects and/or side effects of greater severity [1],[5],[6].

More recently, a newer approach for treating EGF-overexpressing cancers has been to use EGF receptor inhibitors (EGFRIs). The use of EGFRIs has increased the efficacy of drug therapy in treating EGF-overexpressing cancers and have also helped

reduce systemic side effects of treatment. However, EGFRIs may still cause significant systemic side effects, including skin, hair, nail, and mucosal side effects, as they still act generally in the body. Additionally, EGFRIs have not eliminated the need for conventional treatments such as radiation therapy [7],[8],[9].

To achieve the goal of maximizing the effectiveness of treatment while simultaneously minimizing undesirable systemic side effects, the ideal solution would be to use targeted drug delivery to release drugs specifically in the neighborhood of EGF-overexpressing tumors [10]. As the incidence of cancers continues to rise as overall life expectancies increase, the development of such targeted clinical treatment methods for EGF-overexpressing cancers is of critical importance.

One method for targeted drug delivery that has been researched and used extensively is to use drug-encapsulating liposomes triggered by such factors as ultrasound [11],[12]. However, drug-encapsulating liposomes triggered by such factors as ultrasound are generally attendant with the inconvenience and cost associated with the use of external medical equipment (e.g., an ultrasound machine). Also, it is not always clear (e.g., in the case of metastatic tumors) where the triggering factor (e.g., ultrasound waves) should be aimed when the tumors' precise locations are unknown.

Since the goal is to treat EGF-overexpressing cancers, the ideal solution would be to develop drug-encapsulating liposomes triggered by abnormal amounts of EGF (i.e., EGF-sensitive liposomes).

With the interdisciplinary application of principles from biology, chemistry, mathematics, and chemical engineering, functional EGF-sensitive drug-encapsulating liposomes have been successfully developed *in vitro*, and additionally, quantitative mathematical models that can help optimize (drug-encapsulating) liposomes in general have been developed.

This paper includes several main parts. First, the relevant experimental methods for preparation and characterization of EGF-sensitive drug-encapsulating liposomes are presented in Chapter 2. The experimental results are then analyzed and discussed in Chapter 3. Chapter 4 presents quantitative mathematical models characterizing key rate processes associated with industrial liposome preparation and the *in vivo* behavior of liposomes. Finally, Chapters 5 and 6 discuss the ramifications of the experimental and modeling studies presented.

Chapter 2

Materials and Methods

2.a Epidermal Growth Factor (EGF) Receptor Modification

p-toluic acid (Alfa Aesar) was added at a molar ratio of 1:1 to 1 µg EGF receptor (Invitrogen; supplied in 50 mM Tris-HCl, 150 mM NaCl, 0.5 mM EDTA, 0.02% Triton X-100, 2 mM DTT, 50% glycerol; buffered at pH 7.5). The p-toluic acid and EGF receptor were then crosslinked with an EDC/NHS system (Pierce).

Independently, in a separate container, methyl-PEG_4-NHS ester (Pierce), an NHS-activated polyethylene glycol compound, was added at a molar ratio of 1:1 to 1 µg EGF receptor (supplied in 50 mM Tris-HCl, 150 mM NaCl, 0.5 mM EDTA, 0.02% Triton X-100, 2 mM DTT, 50% glycerol; buffered at pH 7.5); the solution was then thoroughly mixed.

The two independently prepared solutions above were then combined and thoroughly mixed to obtain a single solution containing both types of modified EGF receptors (i.e., toluic acid-crosslinked EGF receptors and methyl-capped polyethylene glycol-crosslinked EGF receptors) [13],[14].

2.b Liposome Preparation

0.2 mg egg phosphatidylcholine (Lipoid) was added to a polypropylene tube (BD Falcon); 1.5 ml chloroform (Mallinckrodt Baker) was then added to dissolve the egg phosphatidylcholine. The chloroform was then evaporated under a stream of nitrogen (Airgas), leaving a thin lipid film on the walls of the polypropylene tube which was redried twice under nitrogen to remove traces of residual solvent [15],[16],[17],[18],[19].

The dried lipid film was rehydrated in 0.2 ml Tris-buffered saline (Invitrogen; 20 mM Tris, 150 mM NaCl, pH 7.4) containing 50 mM octyl-β-glucoside (Pierce); the rehydrated solution was then thoroughly mixed by vortexing. The mixed rehydrated solution was dialyzed for 36 h against three changes of buffer (consisting of Tris-buffered

saline, 30 mM benzamidine, HCl (Calbiochem), and 0.1 mM phenylmethylsulfonyl fluoride (Pierce)) to remove the detergent, allowing liposomes to form [15],[16],[18].

The resulting turbid liposome solution was mixed with sucrose (EMD Biosciences) to 40% (weight/volume), applied at the bottom of a sucrose gradient (consisting of 0.5 ml 40% sucrose solution, 1.5 ml 20% sucrose solution, and 1.5 ml 5% sucrose solution, in that order), and then centrifuged at 40,000 g for 3 h to remove residual detergent traces. Finally, fractions were collected from the top of the sucrose gradient [15],[16].

2.c Drug-Encapsulating Liposome Preparation

Drug-encapsulating liposomes were prepared by adding 1 mg/ml actinomycin D (EMD Biosciences), 14-hydroxydaunomycin, HCl (Calbiochem), or 4-amino-10-methylfolic acid (Calbiochem) to the rehydrated lipid solution prepared above (see the section above titled *Liposome Preparation*), prior to the vortexing step [16].

2.d Epidermal Growth Factor (EGF)-Sensitive Liposome Preparation

EGF-sensitive liposomes were prepared by adding the combined modified EGF receptor solution prepared above (see the section above titled *Epidermal Growth Factor (EGF) Receptor Modification*) to the rehydrated lipid solution prepared above (see the section above titled *Liposome Preparation*), prior to the vortexing step [15],[17].

2.e Modified Epidermal Growth Factor (EGF) Receptor Binding Assay

The EGF-binding capability of modified EGF receptors prepared above (see the section above titled *Epidermal Growth Factor (EGF) Receptor Modification*) was assessed using radiolabeled [^{125}I]EGF (PerkinElmer), as described [15].

2.f Modified Epidermal Growth Factor (EGF) Receptor Dimerization Assay

The dimerization capability of modified EGF receptors prepared above (see the section above titled *Epidermal Growth Factor (EGF) Receptor Modification*) was

assessed using SDS-PAGE with Coomassie blue staining (Invitrogen), as described [20],[21],[22].

2.g Drug Release (*In Vitro*) Assay

At various time points, free (unencapsulated) drug molecules and drug-encapsulating liposomes (encapsulated drug molecules) in a drug-encapsulating liposome sample were phase separated; each time, a small (30 μl) aliquot was removed from each solution phase. The change in unencapsulated drug concentration in the sample over time was determined using ^{1}H NMR spectroscopy (400 MHz, $CDCl_3$) or UV-visible spectroscopy [23],[24],[25],[26],[27].

2.h Liposome Size/Stability Assay

The effective diameter of EGF-sensitive liposomes was assessed at various points in the liposomes' lifetime using dynamic light scattering (Brookhaven ZetaPALS) [28].

Chapter 3

Results

The main goal was to develop modified epidermal growth factor (EGF) receptor-bearing drug-encapsulating liposomes sensitive and responsive to EGF in the extraliposomal solution. After these drug-encapsulating liposomes were successfully developed, the goals were to, firstly, verify that said liposomes were sensitive and responsive to abnormal levels of EGF in the extraliposomal solution and, secondly, assess the specificity of said liposomes' sensitivity to EGF (relative to other growth factors). Additional goals were to characterize the effective diameter and stability of said liposomes, to assess the EGF binding activity of the modified EGF receptors, and to characterize the dimerization activity of the modified EGF receptors.

3.a Modified EGF Receptor-Bearing Drug-Encapsulating Liposomes

The initial goal of this study was to assess whether the modified EGF receptor-bearing drug-encapsulating liposomes (prepared as described in *Materials and Methods*) were sensitive and responsive to abnormal levels of EGF in the extraliposomal solution. The secondary goal was to assess whether these liposomes were sensitive specifically to EGF or if they would also undesirably respond significantly to other growth factors, such as vascular endothelial growth factor (VEGF) or fibroblast growth factor (FGF), in the extraliposomal solution. It was found that the liposomes were uniquely triggered by EGF, since only EGF could bind with high affinity to the EGF receptors.

To assess whether the liposomes were sensitive and responsive to EGF, modified EGF receptor-bearing actinomycin D-encapsulating liposomes were formulated and ^{1}H NMR spectroscopy was used to monitor drug release from said liposomes when EGF was added or no EGF was added to the extraliposomal solution. The change in the ^{1}H NMR absorption spectra between 7.5-8.0 ppm over time of each sample was recorded, and the results from each sample were compared [24].

Due to differences in density, buffered saline liposome solutions naturally segregated into three distinct phases at equilibrium: a top liposomal solution phase containing, largely, intact liposomes as well as some free phosphatidylcholine lipid; a middle free phosphatidylcholine solution phase containing, largely, free lipid as well as some free/released drug (for drug-encapsulating liposome solutions); and a lower clumped phosphatidylcholine phase containing, largely, clumped phosphatidylcholine lipid as well as free/released drug (for drug-encapsulating liposome solutions).

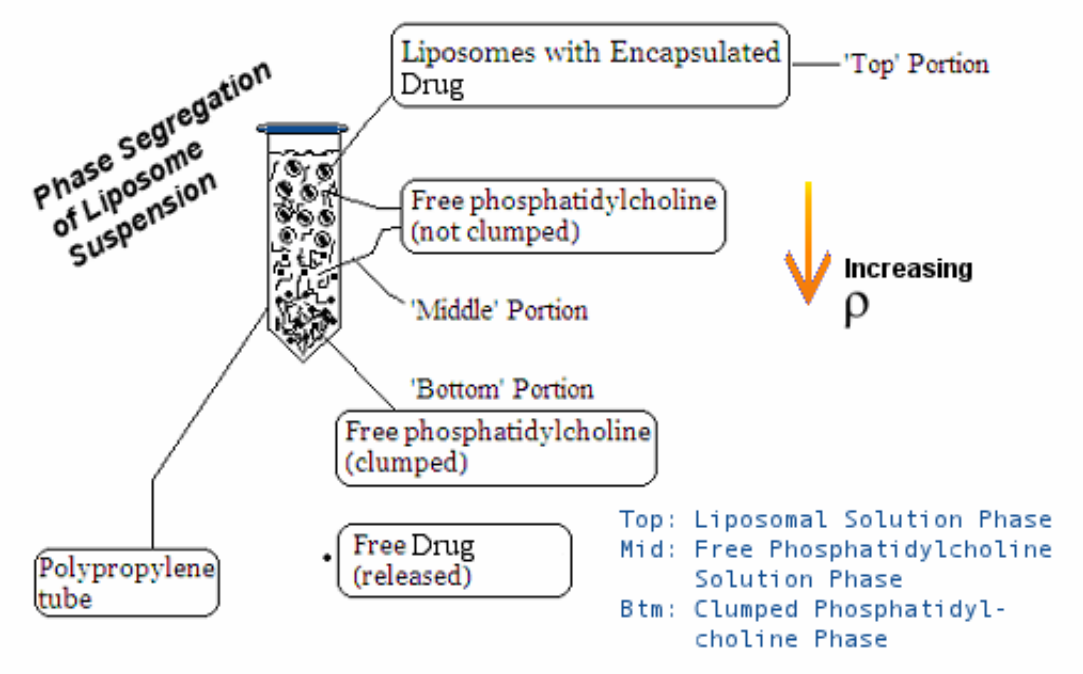

Figure 1 – Schematic showing phase segregation of a drug-encapsulating liposome suspension.

For both the experimental (actinomycin D-encapsulating liposomes with EGF added to the extraliposomal solution) and control (actinomycin D-encapsulating liposomes with no EGF added) samples, the absorption between 7.5-8.0 ppm of samples drawn from the free phosphatidylcholine solution phase increased from 0 d to 7 d after the beginning of the experiment (i.e., the time of addition of EGF, in the case of the experimental sample). However, the absorption of samples drawn from the free

phosphatidylcholine solution phase did not increase at the same rate in the experimental and control samples.

At the beginning of the experiment, the absorption of samples drawn from the free phosphatidylcholine solution phase in the experimental sample was equal to the absorption of samples drawn from the free phosphatidylcholine solution phase in the control sample (see Figure 2, below). By 7 d after the beginning of the experiment, the absorption of samples drawn from the free phosphatidylcholine solution phase in the experimental sample was ~12% more than the absorption of samples drawn from the free phosphatidylcholine solution phase in the control sample.

In a given sample, when encapsulated actinomycin D (i.e., actinomycin D in liposomes) was released or leaked, the freed actinomycin D segregated from the liposomal solution phase into the lower phases (including the free phosphatidylcholine solution phase) of said sample. An increase in the amount/concentration of actinomycin D in the free phosphatidylcholine solution phase of a given sample resulted in a proportional increase in the absorption of samples drawn from said phase of said sample. Hence, a greater increase in absorption over a given amount of time (i.e., a higher rate of increase in absorption) translated to a larger amount of encapsulated actinomycin D being released over said amount of time (i.e., a higher rate of release of encapsulated drug).

In the case of the control sample, there was a low intrinsic rate of leakage of encapsulated drug, resulting in a low rate of increase in absorption. In the case of the experimental sample, there was a higher, EGF-induced rate of release of encapsulated drug, resulting in a somewhat (~12%) higher rate of increase in absorption. Hence, the experimental results indicated that modified EGF receptor-bearing liposomes are (at least somewhat) sensitive and responsive to abnormal levels of EGF in the extraliposomal solution. Further experiments should be conducted to more precisely characterize the EGF sensitivity of these liposomes.

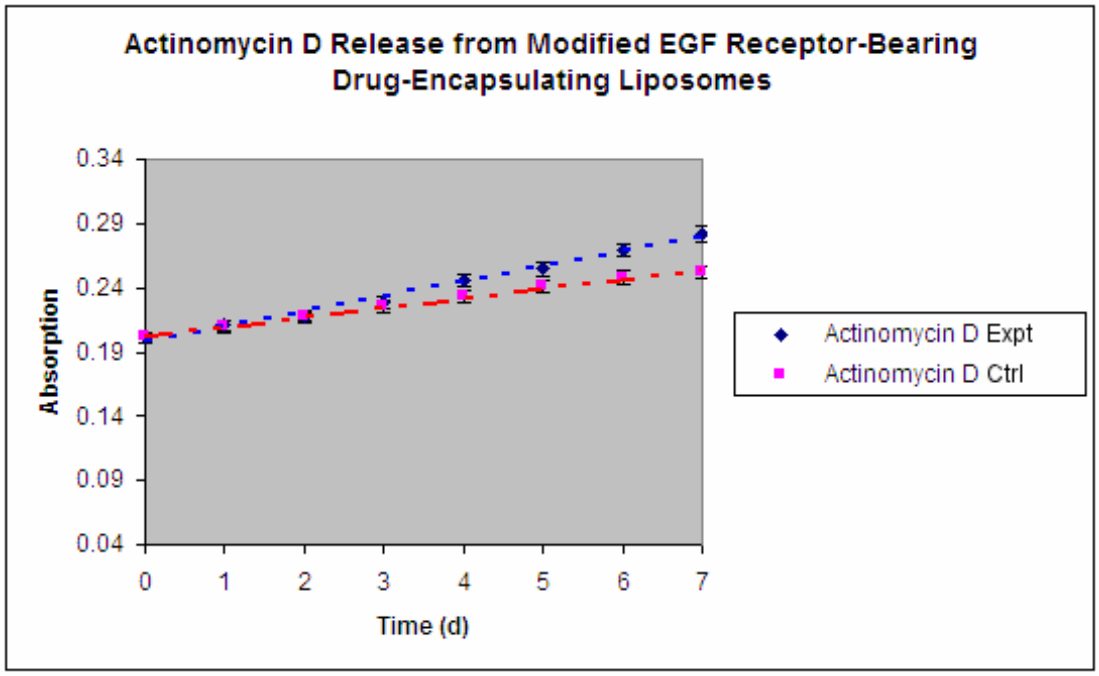

Figure 2 – Actinomycin D release from modified EGF receptor-bearing drug-encapsulating liposomes. The absorption is shown as a function of time. Release was measured at an incubation temperature of 25 °C. Aliquots for ^{1}H NMR spectroscopy were taken from experimental and control samples at various time points as previously described.

To assess whether the liposomes were sensitive *specifically* to EGF or not, doxorubicin-encapsulating EGF-sensitive liposomes were formulated and UV-visible spectroscopy was used to monitor drug release from said liposomes when EGF was added, no EGF was added, VEGF was added, or FGF was added to the extraliposomal solution. An additional control involved using UV-visible spectroscopy to monitor non-drug-encapsulating EGF-sensitive liposomes with EGF added to the extraliposomal solution. The change in the UV-visible absorption spectra at 490 nm λ over time of each sample was recorded, and the results from each sample were compared [25],[26].

For the experimental sample (doxorubicin-encapsulating EGF-sensitive liposomes with EGF added to the extraliposomal solution), the absorbance of samples drawn from the liposomal solution phase decreased from 0 min to 30 min after the beginning of the

experiment (i.e., the time of addition of EGF), and the absorbance of samples drawn from the free phosphatidylcholine solution phase increased from 0 min to 30 min after the beginning of the experiment (i.e., the time of addition of EGF).

For the control samples (doxorubicin-encapsulating EGF-sensitive liposomes with no EGF added, doxorubicin-encapsulating EGF-sensitive liposomes with VEGF or FGF added to the extraliposomal solution, or non-doxorubicin-encapsulating EGF-sensitive liposomes with EGF added to the extraliposomal solution), the absorbance of samples drawn from the liposomal solution phase, as well as the absorbance of samples drawn from the free phosphatidylcholine solution phase, increased from 0 min to 30 min after the beginning of the experiment (i.e., the time of addition of EGF, FGF, or VEGF, if any growth factor was added to the extraliposomal solution).

In a given sample, when encapsulated doxorubicin (i.e., doxorubicin in liposomes) was released, the freed doxorubicin segregated from the liposomal solution phase into the lower phases (including the free phosphatidylcholine solution phase) of said sample. A decrease in the amount/concentration of doxorubicin in the liposomal solution phase of a given sample resulted in a proportional decrease in the absorbance of samples drawn from said phase of said sample. Also, in any given sample, there was a low intrinsic amount of liposome destabilization that resulted in lipids adopting less-ordered arrangements. Thus, in the absence of a significant decrease in the amount/concentration of doxorubicin in the liposomal solution phase of a given sample, a low intrinsic amount of liposome destabilization resulted in an increase in the absorbance of samples drawn from said phase of said sample. Hence, a net decrease in absorbance translated to a significant amount of encapsulated doxorubicin being released.

In the case of the control samples, there was no significant release of encapsulated drug, resulting in an increase in absorbance of liposomal solution phase samples. In the case of the experimental sample, there was a greater, EGF-induced release of encapsulated drug, resulting in a decrease in absorbance of liposomal solution phase samples. Hence, the experimental results indicated that EGF-sensitive liposomes are

specifically sensitive to EGF. Further experiments should be conducted to more precisely characterize the specificity and sensitivity of these liposomes.

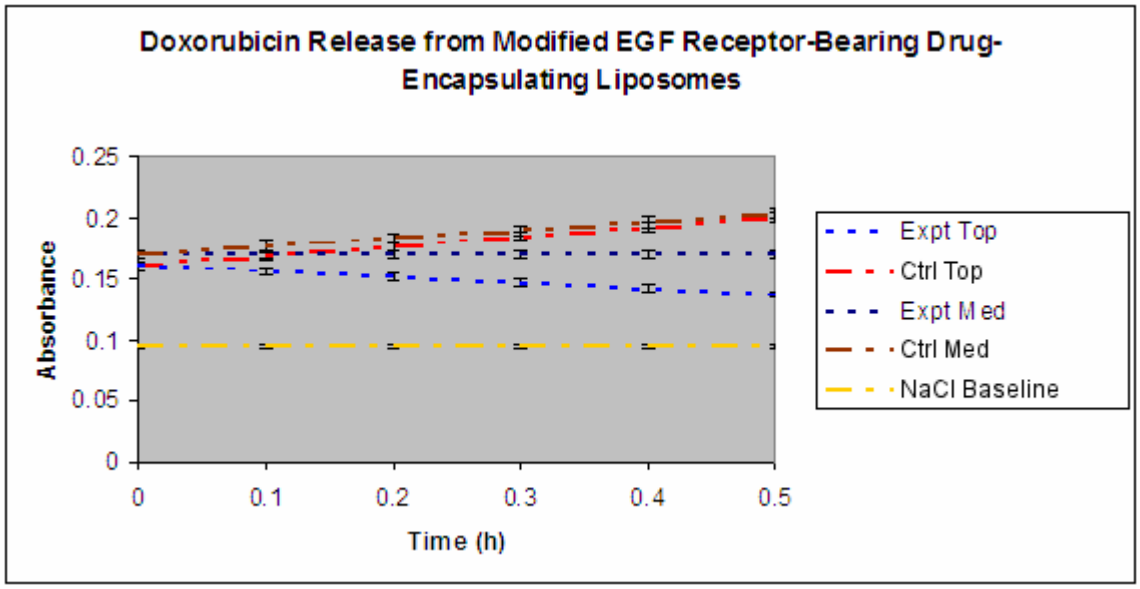

Figure 3 – Doxorubicin release from modified EGF receptor-bearing drug-encapsulating liposomes. The absorbance is shown as a function of time. Release was measured at an incubation temperature of 25 °C. Aliquots for UV-visible spectroscopy were taken from experimental and control samples at various time points as previously described.

3.b Particle Sizing of EGF-Sensitive Liposomes

The goal of this study was to characterize the particle size and stability of the EGF-sensitive liposomes. It was found that the liposomes had an effective diameter of ~630 nm while inert. It was additionally found that the liposomes rapidly became unstable after being exposed to an abnormal concentration of EGF in the extraliposomal solution.

To assess the particle size and stability of the liposomes, EGF-sensitive liposomes were formulated and dynamic light scattering (DLS) was used to determine and monitor the particle size of the liposomes in buffered saline solution when EGF was added or no EGF was added to the extraliposomal solution. The particle size over time of the liposomes in each sample was determined and recorded.

The liposomes in the experimental sample initially had an effective diameter of ~630 nm but rapidly became unstable (O(min)) after the addition of EGF to the solution, forming unordered lipid clumps with an effective diameter of ~20 μm. The liposomes in the control sample (no EGF added to solution) initially had an effective diameter of ~630 nm and maintained this effective diameter over 24 hr.

Brookhaven Instruments Corp.
Brookhaven Instruments - ZetaPALS Particle Sizing Software Ver. 2.34

Date: Jun 30, 2007
Time: 16:28:12
Batch: 0

Sample ID **methotrexate-encapsulating liposomes (Combined)**
Operator ID **ALBERT**
Notes

Measurement Parameters:

Temperature	= 25.0 deg. C	Runs Completed	= 3
Liquid	= Aqueous	Run Duration	= 00:01:00
Viscosity	= 0.890 cP	Total Elapsed Time	= 00:03:00
Ref.Index Fluid	= 1.330	Average Count Rate	= 127.5 kcps
Angle	= 90.00	Ref.Index Real	= 1.590
Wavelength	= 676.0 nm	Ref.Index Imag	= 0.000
		Dust Filter	= Off

methotrexate-encapsulating liposomes (Combined)

Effective Diameter: 636.9 nm
Polydispersity: 0.262
Sample Quality: 9.7
Elapsed Time: 00:03:00

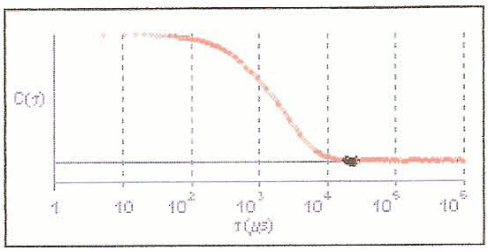

Correlation Function

Run	Eff. Diam. (nm)	Half Width (nm)	Polydispersity	Sample Quality
1	614.6	326.8	0.283	4.9
2	629.7	323.6	0.264	9.0
3	668.6	335.5	0.252	8.2
Mean	637.6	328.6	0.266	7.3
Std. Error	16.1	3.6	0.009	1.3
Combined	636.9	325.7	0.262	9.7

Figure 4 – Inert size of the EGF-sensitive liposomes.

Brookhaven Instruments Corp.
Brookhaven Instruments - ZetaPALS Particle Sizing Software Ver. 2.34

Date: Jun 30, 2007
Time: 16:35:44
Batch: 0

Sample ID **met liposomes clumps (Combined)**
Operator ID **ALBERT**
Notes

Measurement Parameters:

Temperature	= 25.0 deg. C	Runs Completed	= 3
Liquid	= Aqueous	Run Duration	= 00:01:00
Viscosity	= 0.890 cP	Total Elapsed Time	= 00:03:00
Ref.Index Fluid	= 1.330	Average Count Rate	= 33.4 kcps
Angle	= 90.00	Ref.Index Real	= 1.590
Wavelength	= 676.0 nm	Ref.Index Imag	= 0.000
		Dust Filter	= Off

met liposomes clumps (Combined)

Effective Diameter: 20795.9 nm
Polydispersity: 0.442
Sample Quality: 0.0
Elapsed Time: 00:03:00

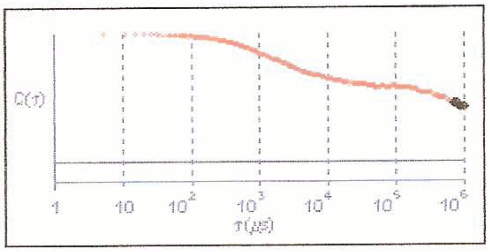

Correlation Function

Run	Eff. Diam. (nm)	Half Width (nm)	Polydispersity	Sample Quality
1	446.9	254.9	0.325	0.0
2	1328.9	868.0	0.427	0.0
3	18290.8	12187.7	0.444	0.0
Mean	6688.9	4436.9	0.399	0.0
Std. Error	5806.5	3879.5	0.037	0.0
Combined	20795.9	13833.3	0.442	0.0

Figure 5 – Destabilized size of the clumped EGF-sensitive liposomes.

3.c Binding Activity of Modified EGF Receptors

The aim of this study was to verify that the liposome-borne modified epidermal growth factor (EGF) receptors on EGF-sensitive liposomes were able to successfully bind to EGF with high affinity. It was found that said modified EGF receptors were indeed able to bind to EGF with high affinity.

To assess whether the liposome-borne modified EGF receptors were able to bind to EGF with high affinity, non-drug-encapsulating liposomes were formulated and liquid scintillation counting was used to determine radiolabeled EGF ([^{125}I]EGF) distribution in liposome suspensions (which were prepared as previously described) when EGF-sensitive liposomes (expt) or non-EGF-sensitive liposomes (ctrl) were used. Unbound ligands were removed by density gradient centrifugation to ensure accuracy of results. The radioactivity of each sample was recorded, and the results from each sample were compared [15].

The experimental sample (EGF-sensitive liposomes with [^{125}I]EGF added) displayed specific binding of [^{125}I]EGF. The control sample (non-EGF-sensitive liposomes with [^{125}I]EGF added) did not display binding of [^{125}I]EGF.

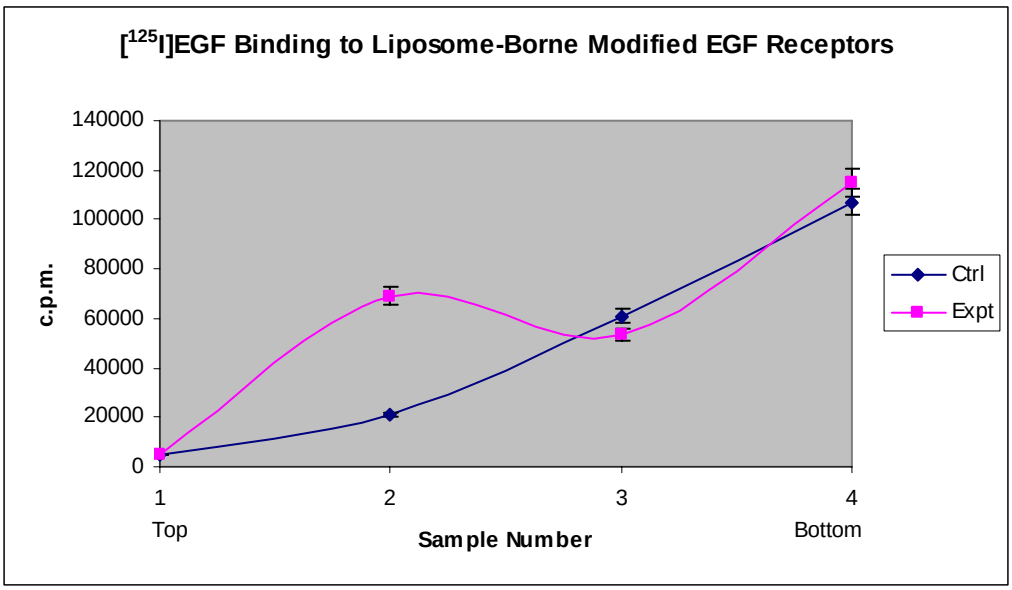

Figure 6 – [^{125}I]EGF binding to liposome-borne modified EGF receptors. The c.p.m. is shown as a function of sample number. Binding assays were done as previously described on EGF-sensitive liposomes (expt) and non-EGF-sensitive liposomes (ctrl).

3.d Dimerization Activity of Modified EGF Receptors

The aim of this study was to verify that the modified epidermal growth factor (EGF) receptors were able to dimerize in the presence of EGF. It was found that said modified EGF receptors were indeed able to dimerize in the presence of EGF.

To assess whether the modified EGF receptors were able to dimerize in the presence of EGF, modified EGF receptors were formulated (as described in *Materials and Methods*) and SDS-PAGE with Coomassie blue staining was used to determine whether modified EGF receptors dimerize upon binding of EGF. Modified (expt) or unmodified (ctrl) EGF receptors and EGF were incubated together and subsequently treated with DSS in order to make EGF-induced dimer formation irreversible. Additional controls involved modified or unmodified EGF receptors in the absence of EGF. The resulting proteins were analyzed using SDS-PAGE, and the results from each sample were compared [22].

Both modified and unmodified EGF receptors formed dimers in the presence of EGF and did not dimerize in the absence of EGF.

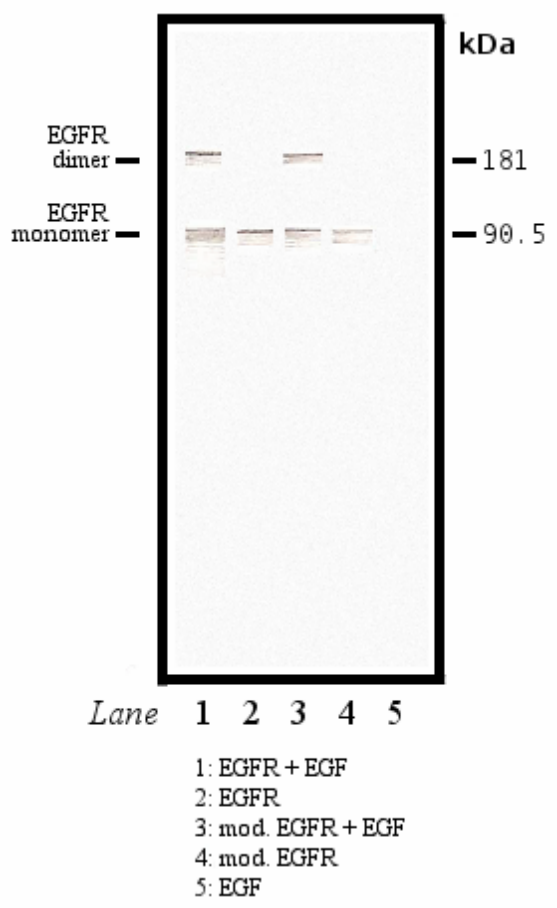

Figure 7 – Modified EGF receptor dimerization. Dimerization assays were performed for modified EGF receptors in the presence of EGF (expt, lane 3), modified EGF receptors only (ctrl, lane 4), unmodified EGF receptors in the presence of EGF (ctrl, lane 1), unmodified EGF receptors only (ctrl, lane 2), and EGF only (baseline ctrl, lane 5).

Chapter 4

Mathematical Models

After drug-encapsulating prototype EGF-sensitive liposomes were developed and experimentally assessed *in vitro*, the goal was to develop mathematical models to quantitatively analyze and describe key chemical processes associated with the industrial production and *in vivo* behavior of liposomes.

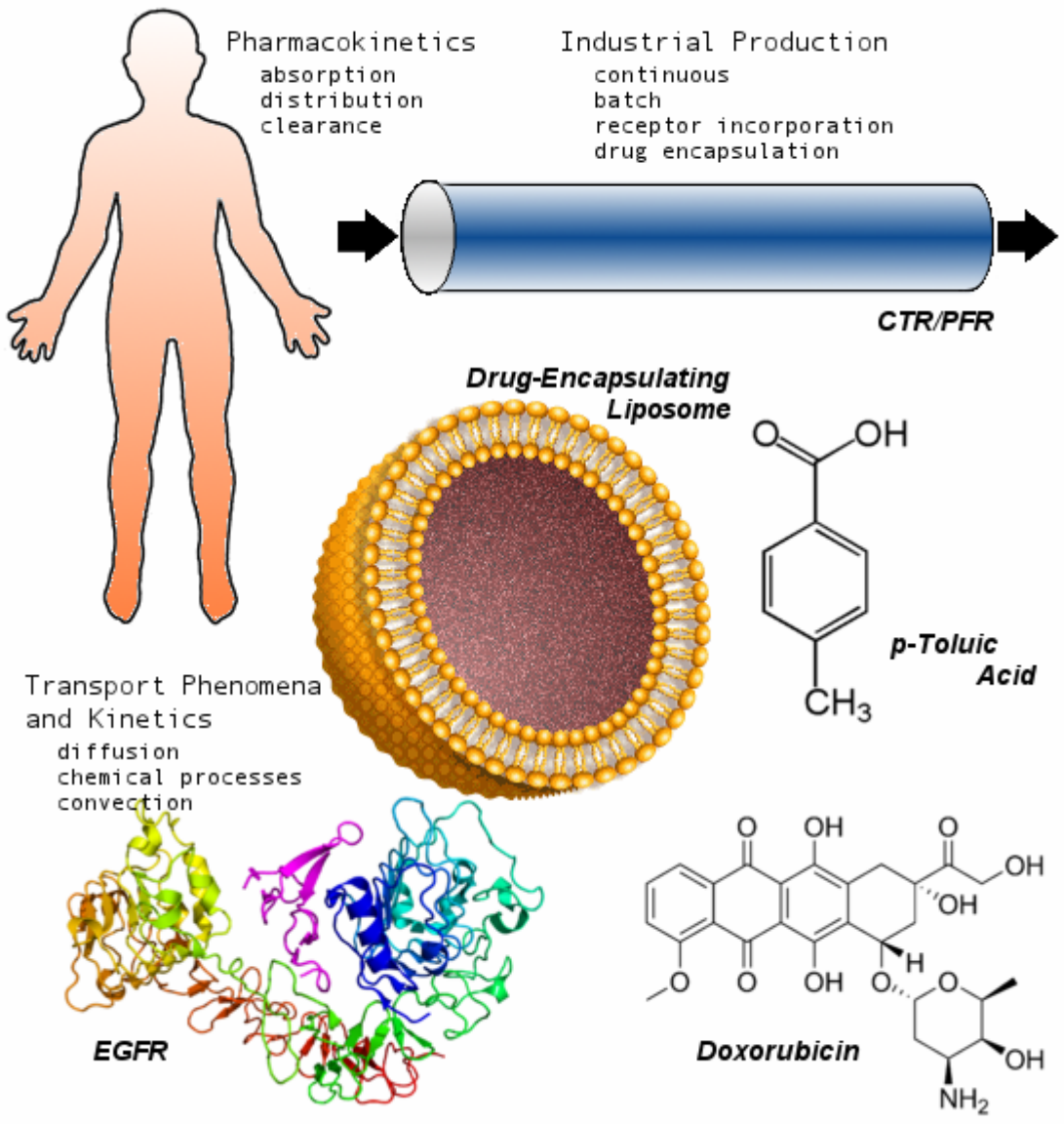

Figure 8 – Schematic depicting various chemical processes associated with liposomes that can be simulated by quantitative mathematical modeling.

4.a Model I: Drug Leakage from Multilamellar Liposome Vesicles (MLVs)

Quantitative Mathematical Model I aims to model the rate process of drug leakage from drug-encapsulating liposomes, specifically MLVs. MLVs (instead of basic unilamellar liposome vesicles (ULVs); see Figure 8) were selected for modeling since their general configuration inherently minimizes drug leakage. As demonstrated below, given just four basic parameters, Quantitative Mathematical Model I allows one to quantitatively model and predict drug leakage over time for many drugs and many homogeneous MLV compositions.

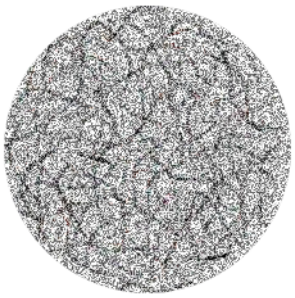

Figure 9 – Schematic of a typical multilamellar liposome vesicle (MLV).

By the general species conservation equation, the rate of accumulation of species *i* within a specific region is a function of the rates at which said species *i* enters or is formed within said specific region.

$$\frac{\partial C_i}{\partial t} = -\nabla \cdot \mathbf{N}_i + R_i \tag{A.1}$$

where C_i represents the molar concentration of species *i*, $\mathbf{N}_i$ represents the molar flux of species *i* relative to fixed coordinates, and R_i represents the net rate, per unit volume, at which species *i* is formed [29].

In the case of species *i* being a minor component in a pseudobinary liquid solution with constant density ρ and diffusivity D_i, Eq. A.1 can be rewritten using Fick's law as:

$$\frac{DC_i}{Dt} = D_i \nabla^2 C_i + R_i \tag{A.2}$$

In spherical coordinates with no fluid flow and no net rate of formation of species *i*, Eq. A.2 becomes [29]:

$$\frac{\partial C_i}{\partial t} = D_i\left[\frac{1}{r^2}\frac{\partial}{\partial r}\left(r^2\frac{\partial C_i}{\partial r}\right)+\frac{1}{r^2\sin\theta}\frac{\partial}{\partial\theta}\left(\sin\theta\frac{\partial C_i}{\partial\theta}\right)+\frac{1}{r^2\sin^2\theta}\frac{\partial^2 C_i}{\partial\phi^2}\right] \qquad \text{(A.3)}$$

For transient drug leakage from a spherically symmetric, homogeneous drug-encapsulating multilamellar liposome vesicle (MLV) of radius R, we can reduce Eq. A.3 to the following governing partial differential equation (PDE):

$$\frac{\partial C}{\partial t} = D\left[\frac{1}{r^2}\frac{\partial}{\partial r}\left(r^2\frac{\partial C}{\partial r}\right)\right] \qquad \text{(A.4)}$$

where C represents the concentration of the drug within the MLV.

We have initial (IC) and boundary conditions (BCs):

$$0 < r < R \quad t \le 0 \qquad C = C_0 \qquad \text{(A.5)}$$

$$r = 0 \quad t \ge 0 \qquad \frac{\partial C}{\partial r} = 0 \qquad \text{(A.6)}$$

$$r = R \quad t \ge 0 \qquad \frac{\partial C}{\partial r} = -\frac{k_C}{D}C \qquad \text{(A.7)}$$

where k_C represents the mass transfer coefficient of the drug [29].

Scaling, we define the following dimensionless variables:

$$\eta = \frac{r}{R} \qquad \theta' = \frac{C}{C_0} \qquad \tau = \frac{D}{R^2}t \qquad \text{(A.8)}$$

Nondimensionalizing Eq. A.4-A.7, then, we obtain:

$$\frac{\partial\theta'}{\partial\tau} = \frac{1}{\eta^2}\frac{\partial}{\partial\eta}\left(\eta^2\frac{\partial\theta'}{\partial\eta}\right) \qquad \text{(A.9)}$$

$$0 < \eta < 1 \quad \tau \le 0 \qquad \theta' = 1 \qquad \text{(A.10)}$$

$$\eta = 0 \quad \tau \ge 0 \qquad \frac{\partial\theta'}{\partial\eta} = 0 \qquad \text{(A.11)}$$

$$\eta = 1 \quad \tau \ge 0 \qquad \frac{\partial\theta'}{\partial\eta} = -\frac{k_C R}{D}\theta' \qquad \text{(A.12)}$$

We now apply the following transformation:

$$\theta(\eta,\tau) = 1 - \theta'(\eta,\tau) \tag{A.13}$$

Eq. A.9-A.12 now become:

$$\frac{\partial\theta}{\partial\tau} = \frac{1}{\eta^2}\frac{\partial}{\partial\eta}\left(\eta^2\frac{\partial\theta}{\partial\eta}\right) \tag{A.14}$$

$$0 < \eta < 1 \quad \tau \le 0 \qquad \theta = 0 \tag{A.15}$$

$$\eta = 0 \quad \tau \ge 0 \quad \frac{\partial\theta}{\partial\eta} = 0 \tag{A.16}$$

$$\eta = 1 \quad \tau \ge 0 \quad \frac{\partial\theta}{\partial\eta} = \frac{k_C R}{D}(1-\theta) \tag{A.17}$$

Using the finite Fourier transform (FFT) method, we seek a solution of the form:

$$\theta(\eta,\tau) = \sum_{n=1}^{\infty}\theta_n(\tau)\phi_n(\eta) \tag{A.18}$$

The basis functions required are those satisfying Robin boundary conditions [29], specifically:

$$\phi_n(\eta) = \sqrt{2}\left[\frac{1-\frac{k_C R}{D}}{\sin^2\lambda_n - \frac{k_C R}{D}}\right]^{1/2}\frac{\sin(\lambda_n\eta)}{\eta}\,,\ \lambda_n = \left(1-\frac{k_C R}{D}\right)\tan\lambda_n\,, \qquad n = 1, 2, \ldots \tag{A.19}$$

Transforming the time and space derivatives in Eq. A.14, we obtain:

$$\int_0^1 \phi_n\frac{\partial\theta}{\partial\tau}\eta^2 d\eta = \frac{d\theta_n}{d\tau} \tag{A.20}$$

$$\int_0^1 \phi_n\left[\frac{1}{\eta^2}\frac{\partial}{\partial\eta}\left(\eta^2\frac{\partial\theta}{\partial\eta}\right)\right]\eta^2 d\eta = \eta^2\left(\phi_n\frac{\partial\theta}{\partial\eta} - \theta\frac{d\phi_n}{d\eta}\right)_{\eta=0}^{\eta=1} - \lambda_n^2\theta_n \tag{A.21}$$

$$= \sqrt{2}\,\frac{k_C R}{D}\left[\frac{1-\frac{k_C R}{D}}{\sin^2\lambda_n - \frac{k_C R}{D}}\right]^{1/2}\sin\lambda_n - \lambda_n^2\theta_n \tag{A.21, cont'd}$$

The initial condition transforms simply to:

$$\theta_n(0) = 0 \tag{A.22}$$

Accordingly, the complete transformed problem is:

$$\frac{d\theta_n}{d\tau} + \lambda_n^2 \theta_n = \sqrt{2}\,\frac{k_C R}{D}\left[\frac{1-\frac{k_C R}{D}}{\sin^2\lambda_n - \frac{k_C R}{D}}\right]^{1/2} \sin\lambda_n \ , \quad \theta_n(0) = 0 \tag{A.23}$$

The solution of Eq. A.23 is:

$$\theta_n = \sqrt{2}\,\frac{k_C R}{D}\left[\frac{1-\frac{k_C R}{D}}{\sin^2\lambda_n - \frac{k_C R}{D}}\right]^{1/2} \sin\lambda_n \,\frac{\left\{1-\exp\left[-\lambda_n^2\tau\right]\right\}}{\lambda_n^2} \tag{A.24}$$

The overall solution, then, using Eq. A.19 and A.24 in Eq. A.18, is:

$$\theta(\eta,\tau) = \sum_{n=1}^{\infty} 2\,\frac{k_C R}{D}\left[\frac{1-\frac{k_C R}{D}}{\sin^2\lambda_n - \frac{k_C R}{D}}\right] \sin\lambda_n \,\frac{\sin\lambda_n\eta}{\eta}\,\frac{\left\{1-\exp\left[-\lambda_n^2\tau\right]\right\}}{\lambda_n^2} \tag{A.25}$$

Inspection shows that the solution in Eq. A.25 consists of two main parts: a transient part which decays exponentially over time and a time-independent part which represents a steady state achieved as $\tau \to \infty$. Eq. A.25 is hence rewritten more simply using the steady-state solution as:

$$\theta(\eta,\tau) = 1 - \sum_{n=1}^{\infty} 2\,\frac{k_C R}{D}\left[\frac{1-\frac{k_C R}{D}}{\sin^2\lambda_n - \frac{k_C R}{D}}\right] \sin\lambda_n \,\frac{\sin\lambda_n\eta}{\eta}\,\frac{\exp\left[-\lambda_n^2\tau\right]}{\lambda_n^2} \tag{A.26}$$

Finally, using Eq. A.26 in Eq. A.13, we obtain:

$$\theta'(\eta,\tau) = \sum_{n=1}^{\infty} 2\,\frac{k_C R}{D}\left[\frac{1-\frac{k_C R}{D}}{\sin^2\lambda_n - \frac{k_C R}{D}}\right] \sin\lambda_n \,\frac{\sin\lambda_n\eta}{\eta}\,\frac{\exp\left[-\lambda_n^2\tau\right]}{\lambda_n^2} \tag{A.27}$$

$$\lambda_n = \left(1 - \frac{k_C R}{D}\right) \tan \lambda_n \tag{A.19}$$

$$\eta = \frac{r}{R} \qquad \theta' = \frac{C}{C_0} \qquad \tau = \frac{D}{R^2} t \tag{A.8}$$

Eq. A.27, in conjunction with Eq. A.8 and A.19, provides a representation of the concentration C of a given drug in a spherically symmetric, homogeneous drug-encapsulating MLV of radius R as a function of radial position and time. Eq. A.27 hence, given four basic parameters: the initial (post-loading) concentration C_0 of the drug in question in the MLV in question, the diffusivity D of said drug in said MLV, the radius R of said MLV, and the mass transfer coefficient k_C of said drug, allows one to quantitatively model and predict drug leakage over time from drug-encapsulating MLVs for many drug and homogeneous MLV combinations.

Model 1 Assumptions: spherically symmetric, homogeneous MLV; uniformly drug-saturated MLV; Fick's law valid; drug bulk concentration in the blood $C_{bulk,\ blood} = 0$ *compared to drug concentration in the liposome* $C_{liposome}$*; constant parameters (D, R,* k_C*,* ρ*); no reactions*

4.b Model II: Vascular Mass Transfer of Liposomes

Quantitative Mathematical Model II aims to model the rate process of the mass transfer of (drug-encapsulating or non-drug-encapsulating) liposomes in blood vessels. As demonstrated below, given just six basic parameters, Quantitative Mathematical Model II allows one to quantitatively model and predict the vascular mass transfer of many types of liposomes.

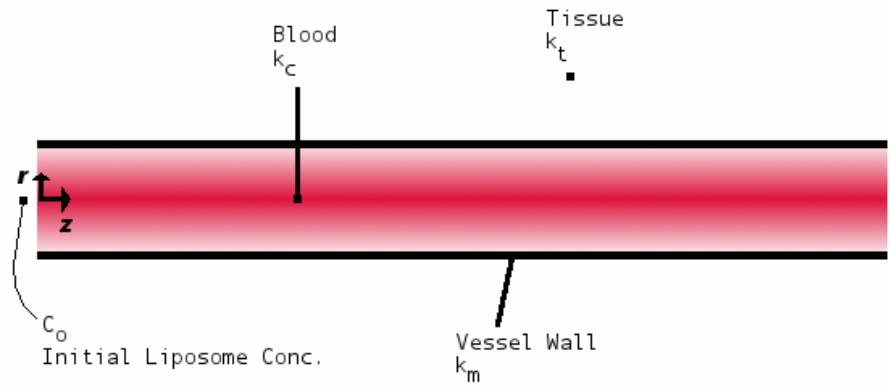

Figure 10 – Schematic of a blood vessel showing mass transfer coefficients.

By the general linear momentum conservation equation, the rate of change of momentum at a material point in a fluid (such as blood) is a function of the body forces and stresses acting on that body of fluid.

$$\rho \frac{D\mathbf{v}}{Dt} = \rho\mathbf{g} + \nabla \cdot \boldsymbol{\sigma} \tag{B.1}$$

where $\boldsymbol{\sigma}$ is the stress tensor [29].

In the case of an incompressible Newtonian fluid with constant viscosity and density, Eq. B.1 can be rearranged and rewritten as the Navier-Stokes equation [29]:

$$\rho \frac{D\mathbf{v}}{Dt} = \rho\mathbf{g} - \nabla P + \mu\nabla^2\mathbf{v} \tag{B.2}$$

or, equivalently,

$$\rho \frac{D\mathbf{v}}{Dt} = -\nabla \mathcal{P} + \mu\nabla^2\mathbf{v} \tag{B.3}$$

where $\mathcal{P}$ is the dynamic pressure [29].

In cylindrical coordinates with fully developed, unidirectional flow, Eq. B.3 reduces to [29]:

$$\rho \frac{\partial v_z}{\partial t} = -\frac{\partial \mathcal{P}}{\partial z} + \mu \left[\frac{1}{r} \frac{\partial}{\partial r} \left(r \frac{\partial v_z}{\partial r} \right) + \frac{1}{r^2} \frac{\partial^2 v_z}{\partial \theta^2} \right] \tag{B.4}$$

which for steady, axisymmetric flow becomes the following ODE:

$$\frac{1}{r} \frac{d}{dr} \left(r \frac{dv_z}{dr} \right) = \frac{1}{\mu} \frac{d\mathcal{P}}{dz} \tag{B.5}$$

Integrating and applying a symmetry boundary condition at $r = 0$, we obtain:

$$r \frac{dv_z}{dr} = \frac{r^2}{2\mu} \frac{d\mathcal{P}}{dz} \tag{B.6}$$

Integrating again and applying a no-slip boundary condition at $r = R$ (where R is the vessel radius), we obtain:

$$v_z(r) = -\frac{R^2}{4\mu} \frac{d\mathcal{P}}{dz} \left\{ 1 - \left(\frac{r}{R} \right)^2 \right\} \tag{B.7}$$

Eq. B.7 can be expressed using the mean velocity U as:

$$v_z(r) = 2U \left\{ 1 - \left(\frac{r}{R} \right)^2 \right\} \tag{B.8}$$

where:

$$U = -\frac{R^2}{8\mu} \frac{d\mathcal{P}}{dz} \tag{B.9}$$

The velocity profile expressed in Eq. B.8 can then be applied in the general species conservation equation for a pseudobinary liquid solution with constant diffusivity, which is:

$$\frac{DC_i}{Dt} = D_i \nabla^2 C_i + R_i \tag{A.2}$$

In cylindrical coordinates, assuming a large Péclet number (neglecting axial diffusion), Eq. A.2 becomes:

$$v_z \frac{\partial C}{\partial z} = D\left\{\frac{1}{r}\frac{\partial}{\partial r}\left(r\frac{\partial C}{\partial r}\right)\right\} \tag{B.10}$$

or, equivalently, using Eq. B.8 in Eq. B.10, we obtain the following governing partial differential equation for liposome distribution in a vessel:

$$2U\left\{1-\left(\frac{r}{R}\right)^2\right\}\frac{\partial C}{\partial z} = D\left\{\frac{1}{r}\frac{\partial}{\partial r}\left(r\frac{\partial C}{\partial r}\right)\right\} \tag{B.11}$$

where C represents the liposome concentration in the vessel.

Integrating Eq. B.10 over r, we obtain [29]:

$$\int_0^R v_z \frac{\partial C}{\partial z} r dr = RD\frac{\partial C}{\partial r}\bigg|_{r=R} = -RN_r \tag{B.12}$$

where N_r represents the liposome flux.

Using the "mixing cup" quantity C_b (see Deen [29]):

$$C_b = \frac{\int_A C v_z dA}{\int_A v_z dA} \tag{B.13}$$

where A is the cross-sectional area, we can rewrite the left-hand side of Eq. B.12 as [29]:

$$\int_0^R v_z \frac{\partial C}{\partial z} r dr = \frac{R^2 U}{2}\frac{dC_b}{dz} \tag{B.14}$$

where U is the mean velocity as given in Eq. B.9.

The liposome flux from the blood to the vessel wall is given by [29]:

$$N_r = k_c\left(C_b - C\big|_{r=R}\right) \tag{B.15}$$

and the liposome flux through the vessel wall is given by [29]:

$$N_r = k_m\left(C\big|_{r=R} - C_t\right) \tag{B.16}$$

where C_t is the liposome concentration in the tissue at the outer vessel wall surface. Finally, the liposome flux in the tissue is written as:

$$N_r = k_t C_t \tag{B.17}$$

Combining Eq. B.12, B.14, and B.15, we obtain [29]:

$$\frac{dC_b}{dz} = -\frac{2k_c}{RU}\left(C_b - C\big|_{r=R}\right) \tag{B.18}$$

The liposome concentration at the inner vessel wall surface $C|_{r=R}$ is now eliminated by equating the three expressions for the flux, Eq. B.15, B.16, and B.17. Rearranging, we obtain:

$$C_b - C\big|_{r=R} = \left(\frac{k_m k_t}{k_c\left(k_m + k_t\right) + k_m k_t}\right) C_b \tag{B.19}$$

Using Eq. B.19 in Eq. B.18, then, the final differential equation for the bulk concentration C_b is:

$$\frac{dC_b}{dz} = -\frac{2}{RU}\left(\frac{k_c k_m k_t}{k_c\left(k_m + k_t\right) + k_m k_t}\right) C_b \tag{B.20}$$

$$C_b(0) = C_o \tag{B.21}$$

where C_o is the initial liposome (inlet) concentration.

The solution of Eq. B.20 is:

$$\frac{C_b}{C_o} = \exp\left[-\frac{2z}{RU}\frac{k_c k_m k_t}{k_c\left(k_m + k_t\right) + k_m k_t}\right] \tag{B.22}$$

$$U = -\frac{R^2}{8\mu}\frac{d\mathcal{P}}{dz} \tag{B.9}$$

Eq. B.22, in conjunction with Eq. B.9, provides a representation of the mass transfer of (drug-encapsulating or non-drug-encapsulating) liposomes in a blood vessel. The model hence, given six basic parameters: the radius R of the vessel, the mean velocity U of fluid flow in said vessel, the initial liposome inlet concentration C_o, and the mass transfer coefficients k_c, k_m, and k_t of the liposomes in the blood, vessel wall, and

tissue space, respectively, allows one to quantitatively model and predict the mass transfer of liposomes in a blood vessel as a function of axial position for many types of liposomes.

The above model can be extended by using first principles to compute the mass transfer coefficient k_c (see references [29],[47],[48]).

*Model 2 Assumptions: incompressible Newtonian blood; Fick's law valid; fully developed blood flow; unidirectional, axisymmetric blood flow; steady blood flow; large Péclet number (Pe = 2*U*R/D ~ 2*(0.001 m/s)*(5*10^{-6} m)/(10^{-12} m^2/s) = 10^4 >> 1 in a capillary); dΦ/dz = constant; constant parameters (D, R, k_C, k_m, k_t, μ, ρ); no reactions*

4.c Model III: Early Post-Administration Tissue Distribution of Liposomes

Quantitative Mathematical Model III aims to model the rate process of the early post-administration tissue distribution of (drug-encapsulating or non-drug-encapsulating) liposomes. As demonstrated below, given just two basic parameters, Quantitative Mathematical Model III allows one to easily quantitatively model and predict the early tissue spatial and temporal distribution of many types of liposomes.

The following governing partial differential equation (PDE) applies for an instantaneous point source of liposomes (i.e., from an injection):

$$\frac{\partial C}{\partial t} = D\left[\frac{\partial^2 C}{\partial x^2} + \frac{\partial^2 C}{\partial y^2} + \frac{\partial^2 C}{\partial z^2}\right] \tag{C.1}$$

where C represents the liposome concentration [29].

We can also apply conservation of mass to write:

$$s = \int_{-\infty}^{\infty}\int_{-\infty}^{\infty}\int_{-\infty}^{\infty} C\,dx\,dy\,dz \tag{C.2}$$

where s is the total amount of liposomes added (i.e., injected) at $t = 0$ [29].

Applying Eq. C.1-C.2 with the appropriate boundary and initial conditions ($C = 0$ at x, y, and z at $\pm\infty$ and at $t = 0$) and solving per Deen [29]:

$$C = \frac{s}{8(\pi D t)^{3/2}} e^{-\left(x^2+y^2+z^2\right)/4Dt} = \frac{s}{8(\pi D t)^{3/2}} e^{-r^2/4Dt} \tag{C.3}$$

For a continuous point source of liposomes (i.e., from an IV or a drug delivery device), Eq. C.3 can be integrated over time to obtain the corresponding continuous point source solution. For a constant release rate from the point source, the solution is [29]:

$$C = \frac{q}{4\pi D r}\,\mathrm{erfc}\left(\frac{r}{2(Dt)^{1/2}}\right) \tag{C.4}$$

where q is the constant liposome release rate from the IV or drug delivery device.

Eq. C.3 and Eq. C.4, above, provide a representation of the liposome concentration C as a function of elapsed time t and radial position r from the liposome point source for short times (i.e., low values of elapsed time). Eq. C.3 and Eq. C.4 hence, given two basic parameters: the total amount s of liposomes added *or* the liposome release rate q, and the effective diffusivity D of said liposomes, allow one to quantitatively model and predict the early post-administration tissue distribution of liposomes for many types of liposomes.

A similar approach can also be used to formulate a model for continuous liposome release from an implanted bolus. Such a model could be solved numerically via finite element analysis [30].

The MATLAB code in Appendix A can be used (with slight modifications as necessary) to numerically evaluate and graphically portray the liposome concentration C as a function of elapsed time t and radial position r from the liposome point source for a constant liposome release rate q. The code can easily be extended to cover the case of an instantaneous point source.

A plot of the liposome concentration C as a function of elapsed time t at various liposome release rates q is shown in Figure 11, below:

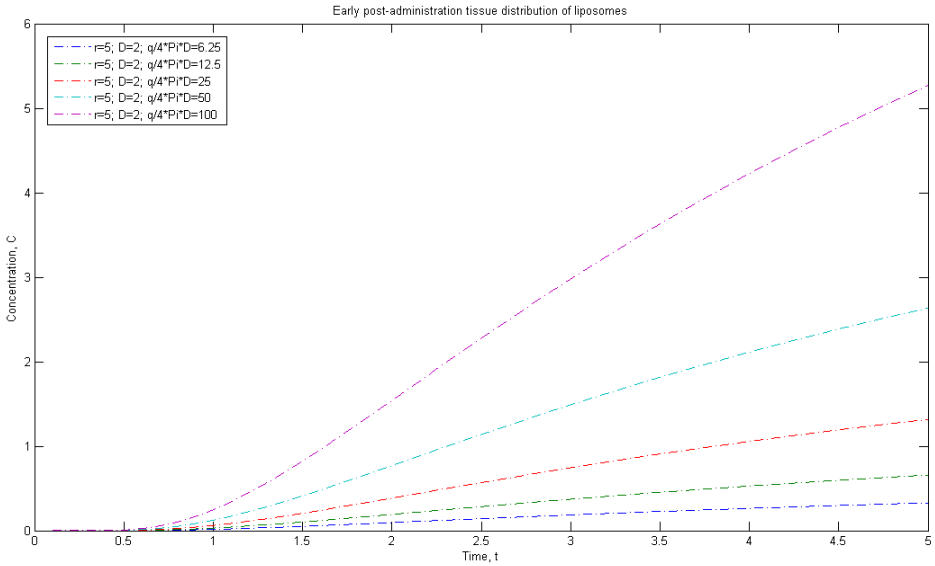

Figure 11 – Early post-administration tissue distribution of liposomes. The liposome concentration is shown as a function of time at various liposome release rates. $D \sim 10^{-12}$ m^2/s

A plot of the liposome concentration C as a function of elapsed time t at various values of radial position r is shown in Figure 12, below:

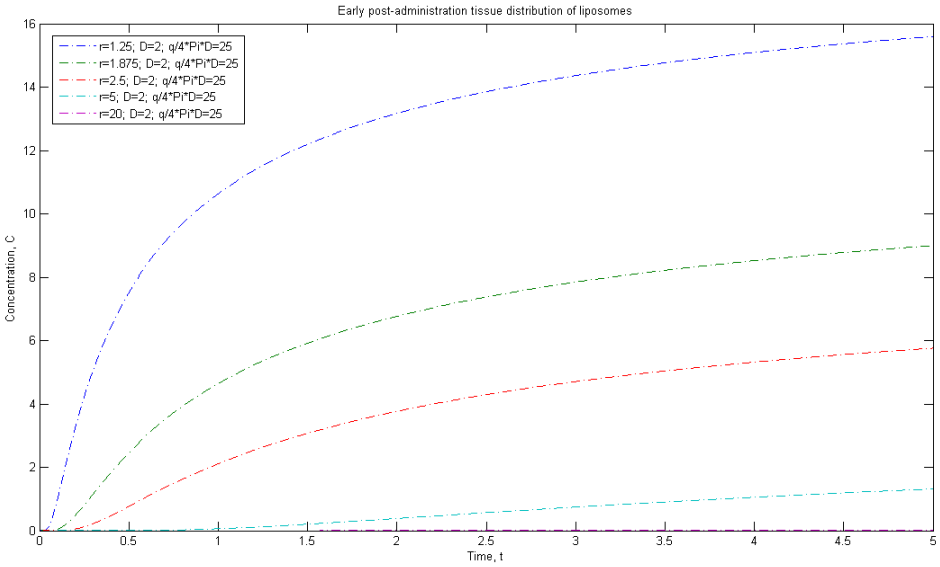

Figure 12 – Early post-administration tissue distribution of liposomes. The liposome concentration is shown as a function of time at various values of radial position.

A plot of the liposome concentration *C* as a function of radial position *r* at various values of elapsed time *t* is shown in Figure 13, below:

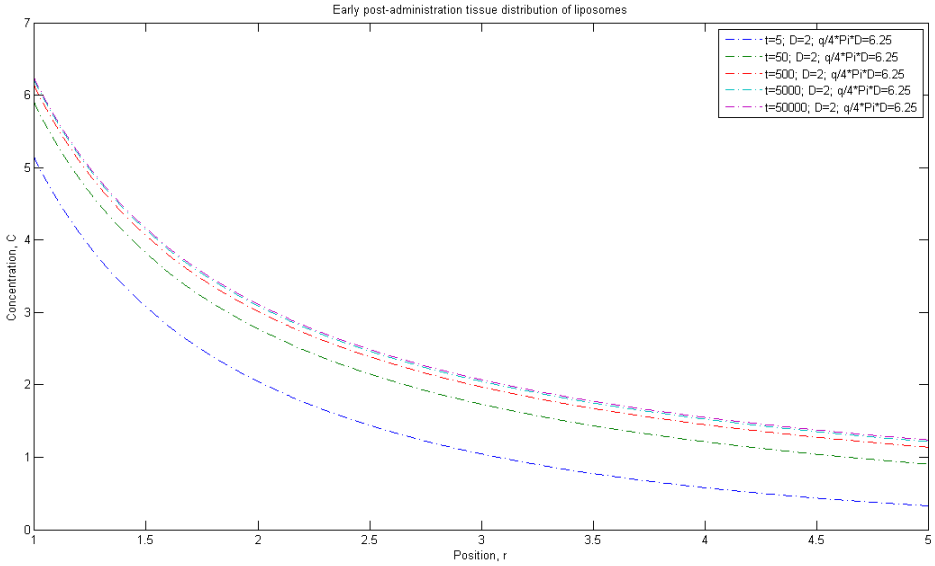

Figure 13 – Early post-administration tissue distribution of liposomes. The liposome concentration is shown as a function of radial position at various values of elapsed time.

Broadly, the plots shown in Figures 11, 12, and 13 above, are consistent with qualitative expectations. At a given radial position, the concentration increases with elapsed time. At a given elapsed time point, the concentration decreases with increasing radial distance from the liposome point source. Also, at a given radial position and elapsed time point, the concentration increases with increasing liposome release rate from the point source.

Model 3 Assumptions: Fick's law valid; no bulk flow; constant parameters (D, q); short (early) times; no reactions

4.d Model IV: Overall Pharmacokinetics of Liposomes

Quantitative Mathematical Model IV aims to model the overall pharmacokinetics of liposomes in the body.

The governing differential equations for a two-compartment open model are [31]:

$$V_P \frac{dC_P}{dt} = -k_{12} C_P V_P + k_{21} C_T V_T - k_C C_P V_P + I \tag{D.1}$$

$$V_T \frac{dC_T}{dt} = k_{12} C_P V_P - k_{21} C_T V_T \tag{D.2}$$

The general solution for the case where $I = 0$ (for an I.V. bolus) is of the form:

$$C_P = Ae^{-\alpha t} + Be^{-\beta t} \tag{D.3}$$

$$k_C = \alpha\beta \frac{(A+B)}{(A\beta + B\alpha)} \tag{D.4}$$

$$k_{12} = AB \frac{(\alpha^2 + \beta^2 - 2\alpha\beta)}{(A+B)(A\beta + B\alpha)} \tag{D.5}$$

$$k_{21} = \frac{(A\beta + B\alpha)}{(A+B)} \tag{D.6}$$

From Eq. D.4, Eq. D.5, and Eq. D.6, above, the effective plasma to tissue (k_{12}), tissue to plasma (k_{21}), and clearance from plasma (k_C) rate constants can be determined from the empirically determined constants A, B, α, and β (which can be evaluated by fitting Eq. D.3 to experimental data on the liposome plasma concentration (C_P) as a function of time). A similar approach can be used with other compartmental models as required by the experimental data. Knowledge of these rate constants (k_{12}, k_{12}, k_C) is helpful in liposome bioavailability and toxicity studies.

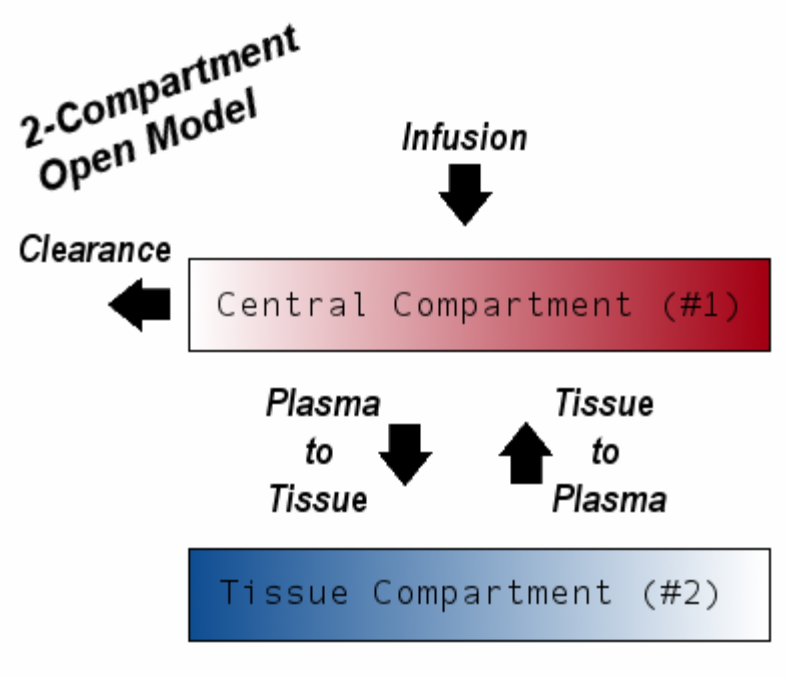

Figure 14 – Schematic showing the basic components of a two-compartment open pharmacokinetic model.

The MATLAB code in Appendix A can be used (with slight modifications as necessary) to fit Eq. D.3 to experimental C_P data using nonlinear least squares regression fitting, as shown in Figure 15, below (experimental data from references [32],[33],[34]):

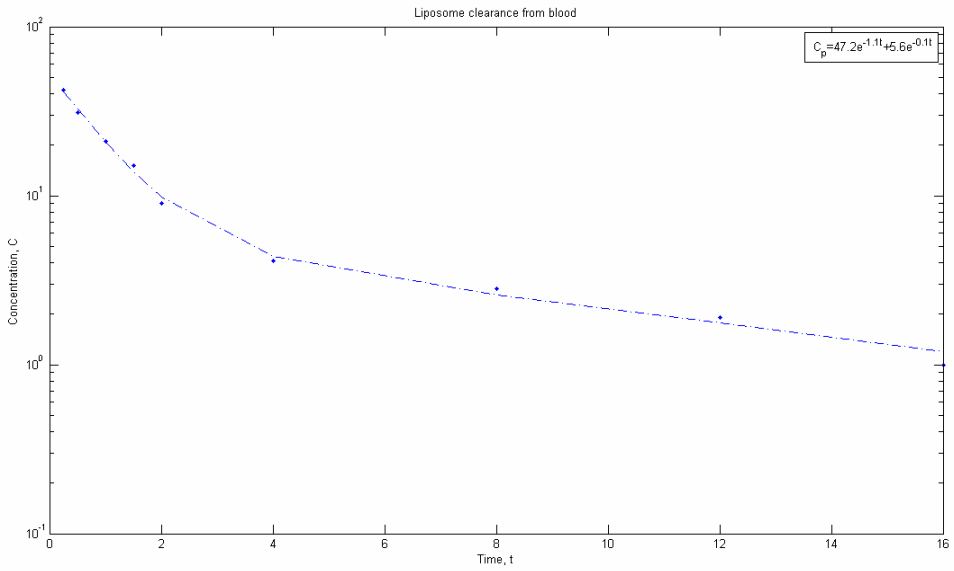

Figure 15 – Liposome clearance from blood. The liposome plasma concentration is shown as a function of time.

Model 4 Assumptions: I = 0 (I.V. bolus); two compartments; constant parameters (k_{12}, k_{21}, k_c, V_P, V_T)

4.e Model V: High-Throughput Production of Liposomes

Quantitative Mathematical Model V aims to model the rate process of continuous, high-throughput production of liposomes in a plug flow reactor (PFR) [35].

The relevant reaction may be represented as [36],[37],[38]:

100 Modified EGF Receptors (MER) (*l*) + 10000 Drug (DRG) (*l*) + 80000 Lipid (LIP) (*s*) → Liposome (DEL) (*l*)

(E.1)

In a plug flow reactor assumed to be ideal, the governing mole balance equation for species *j* is, per Fogler [39]:

$$\frac{dF_j}{dV} = r_j \tag{E.2}$$

Assuming a low feed flow rate *u*, the change in thickness of the deposited lipid film on the walls of the reactor is negligible over short time scales. Hence, Eq. E.2 can be rewritten to evaluate the change in concentration of species *j* C_j with reactor position *L*:

$$\frac{dC_j}{dL} = \frac{r_j}{u} \tag{E.3}$$

For constant radius and flow, the surface reaction rate can be related to changes in the bulk concentrations as follows:

$$\frac{dC_j}{dL} = \frac{d\left(\frac{N_j}{V}\right)}{dL} = \frac{d\left(\frac{N_j}{A}\right)}{dL}\frac{A}{V} = \frac{d\left(\frac{N_j}{A}\right)}{dL}\frac{2\pi r}{\pi r^2} = \frac{d\left(\frac{N_j}{A}\right)}{dL}\frac{2}{r} = \frac{d\left(\frac{N_j}{A}\right)}{dL}\frac{4}{d} \tag{E.4}$$

where N_j represents the number of moles of species *j* and *A* is the area, *V* is the volume, *r* is the radius, and *d* is the diameter of the reactor.

Then, assuming pseudo-second order kinetics with a large excess of deposited lipid (i.e., [LIP] ~ constant for short times) and using the reaction stoichiometry for MER, DRG, and DEL given in Eq. E.1 [36],[37],[38], we obtain the following governing differential equations for the solution-phase species:

$$\frac{d[\mathrm{MER}]}{dL} = -\frac{1}{u}\left(\frac{400}{d}k\right)[\mathrm{MER}][\mathrm{DRG}] \tag{E.5}$$

$$\frac{d[\mathrm{DRG}]}{dL} = -\frac{1}{u}\left(\frac{40000}{d}k\right)[\mathrm{MER}][\mathrm{DRG}] \tag{E.6}$$

$$\frac{d[\mathrm{DEL}]}{dL} = \frac{1}{u}\left(\frac{4}{d}k\right)[\mathrm{MER}][\mathrm{DRG}] \tag{E.7}$$

where k is the reaction rate coefficient.

The MATLAB code in Appendix A can be used (with slight modifications as necessary) to numerically evaluate Eqs. E.5-E.7 and graphically portray the solution-phase species concentrations C as functions of reactor position L, as shown in Figures 16, 17, and 18, below:

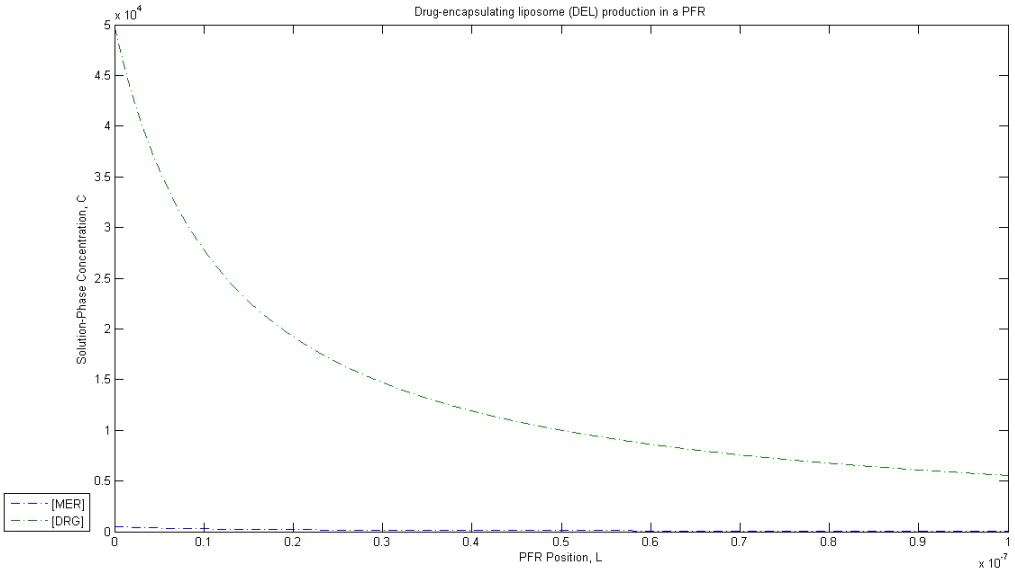

Figure 16 – Drug-encapsulating liposome (DEL) production in a PFR. The solution-phase modified EGF receptor (MER) and drug (DRG) concentrations are shown as functions of reactor position. Initial conditions at reactor inlet: [MER] = 500 arbitrary units (a.u.); [DRG] = 50000 a.u.; [DEL] = 0 a.u.

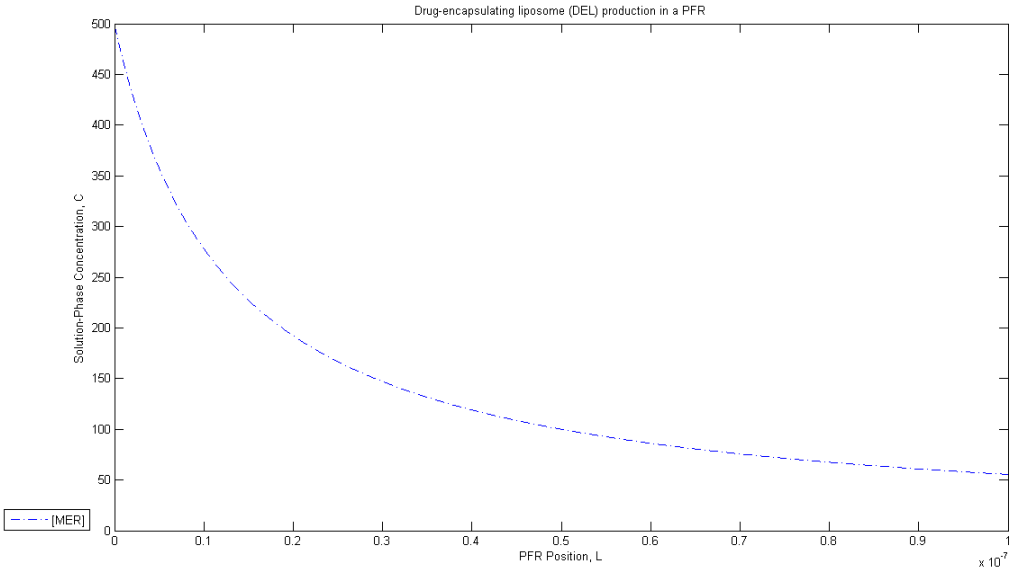

Figure 17 – Drug-encapsulating liposome (DEL) production in a PFR. The solution-phase modified EGF receptor (MER) concentration is shown as a function of reactor position.

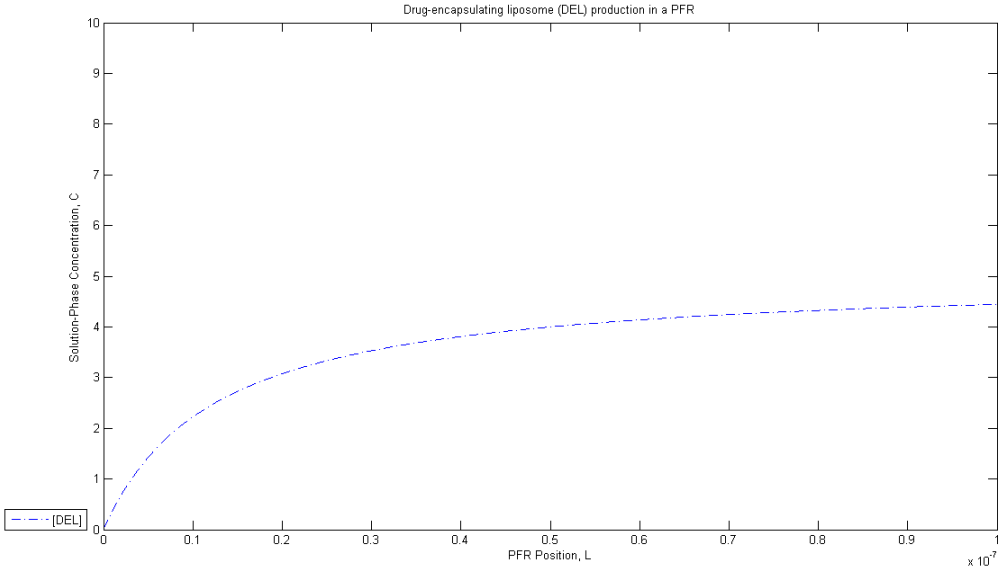

Figure 18 – Drug-encapsulating liposome (DEL) production in a PFR. The solution-phase drug-encapsulating liposome (DEL) concentration is shown as a function of reactor position.

Broadly, the plots shown in Figures 16, 17, and 18, above, are consistent with qualitative expectations. The concentrations of MER and DRG decrease with increasing reactor position, and the concentration of DEL increases correspondingly with increasing reactor position.

Model 5 Assumptions: ideal plug flow reactor; low feed flow rate; short (early) times; adsorption and desorption not rate-limiting; pseudo-second order kinetics; constant parameters (k, r, u)

Chapter 5

Discussion

In summary, this work reports the development of drug-encapsulating EGF-sensitive liposomes for EGF-overexpressing cancer therapies. Experimental methods described herein produce EGF sensitivity in (drug-encapsulating) liposomes by introducing liposome-borne chemically modified EGF receptors. Quantitative mathematical models described herein characterize and describe various critical rate processes associated with drug-encapsulating liposomes and can be used to help design improved drug-encapsulating liposomes. The results represent a significant stepping stone toward the use of drug-encapsulating EGF-sensitive liposomes for EGF-overexpressing cancer therapies in clinical practice.

5.a Some Complications with the *In Vitro* Model

The prototypical experimental setup described herein demonstrates qualitative control of EGF sensitivity in liposomes. The actual *in vivo* processes may be too complicated to allow specific quantification based only on this initial *in vitro* study. The prototypical *in vitro* setup has a number of obvious limitations and departures from *in vivo* physiology. The results are, nevertheless, meaningful because they allow one to characterize the liposomes' basic function in the absence of complicating factors, and they clearly demonstrate the sensitivity of the liposomes to EGF in the extraliposomal solution. Additionally, the results show that the liposomes are able to clearly distinguish between EGF and other growth factors such as VEGF and FGF.

5.b General Liposome Design and Synthesis Optimization

The quantitative mathematical models described herein are potentially of use generally in optimizing the design and synthesis of a broad array of (EGF-sensitive or non-EGF-sensitive) (drug-encapsulating) liposomes. Figures 11, 12, 13, 15, 16, 17, and 18 suggest the applicability of said quantitative mathematical models in assessing the drug leakage, vessel mass transfer, and industrial production rate processes, as well as the *in vivo* pharmacokinetics, of said broad array of (drug-encapsulating) liposomes.

Prior efforts by other researchers in assessing the drug leakage, vessel mass transfer, and industrial production rate processes of liposomes have largely relied on direct experimental testing and analysis [40]. As a result, analysis and testing of novel liposome compositions, configurations, or synthetic methods with the goal of identifying optimal compositions and configurations (to, for example, minimize drug leakage and achieve a favorable mass transfer profile in blood vessels) or optimal synthetic methods (to, for example, maximize the speed and efficiency of liposome production, and hence minimize the liposomes' manufacturing costs) has been somewhat limited.

With the quantitative mathematical models described herein, many more drug-encapsulating liposome compositions, configurations, and synthetic methods could be assessed rapidly and at low cost. In one potential methodology, for instance, quantitative modeling results could be used as a preliminary filter in screening a large number of drug-encapsulating liposome compositions, configurations, or synthetic methods in a high-throughput fashion. Compositions, configurations, or synthetic methods determined to be promising based on the modeling results could then be further assessed with previous evaluation techniques.

With the above potential methodology, optimal compositions, configurations, and synthetic methods that would have gone unidentified with previous evaluation and testing methods might very likely be identified by the application of the quantitative mathematical models described herein in conjunction with previous evaluation techniques. Additionally, other potential methodologies of value involving the quantitative mathematical models described herein may also be devised by those skilled in the art.

Chapter 6

Conclusions

In conclusion, the integrative *in vitro* experiments and quantitative mathematical models presented in this work, utilizing principles and procedures from biology, chemistry, mathematics, and chemical engineering, yield significant scientific and preclinical insights into a novel growth factor-sensitive targeted drug delivery system.

By incorporating liposome-borne chemically modified EGF receptors, liposomes can be made to have EGF sensitivity, allowing drug release to be triggered from drug-encapsulating liposomes by abnormal concentrations of EGF. By quantitatively modeling multiple critical rate processes associated with the function and synthesis of drug-encapsulating liposomes, drug-encapsulating EGF-sensitive liposomes, as well as a broad array of drug-encapsulating liposomes in general, can be assessed and optimized.

This work demonstrates the ability of modified EGF receptor-bearing liposomes to function as EGF-sensitive liposomes *in vitro*. Future research building on this work should involve further preclinical and clinical testing of the *in vivo* efficacy and toxicity of these liposomes.

Appendix A

MATLAB Code

```
function Model_III
clear all;
close all;

%Initialize counter
n=1;

%Set time vector
t=linspace(0.01,5,1000);

%Set parameters
a=6.25;
r=5;
D=2;

while n < 1001
    c(n)=(a/r)*erfc(r/(2*(D*t(n))^(1/2)));
    n=n+1;
end

%Reset counter
n=1;

%Re-set parameters
a=12.5;
r=5;
D=2;

while n < 1001
    c2(n)=(a/r)*erfc(r/(2*(D*t(n))^(1/2)));
    n=n+1;
end

%Reset counter
n=1;

%Re-set parameters
a=25;
r=5;
D=2;

while n < 1001
    c3(n)=(a/r)*erfc(r/(2*(D*t(n))^(1/2)));
    n=n+1;
end

%Reset counter
n=1;
```

```
%Re-set parameters
a=50;
r=5;
D=2;

while n < 1001
    c4(n)=(a/r)*erfc(r/(2*(D*t(n))^(1/2)));
    n=n+1;
end

%Reset counter
n=1;

%Re-set parameters
a=100;
r=5;
D=2;

while n < 1001
    c5(n)=(a/r)*erfc(r/(2*(D*t(n))^(1/2)));
    n=n+1;
end

%Plot figure
figure(1)
plot(t,c,'-.',t,c2,'-.',t,c3,'-.',t,c4,'-.',t,c5,'-.');
title('Early post-administration tissue distribution of liposomes');
xlabel('Time, t');
ylabel('Concentration, C');
legend('r=5; D=2; q/4*Pi*D=6.25','r=5; D=2; q/4*Pi*D=12.5','r=5; D=2;
q/4*Pi*D=25','r=5; D=2; q/4*Pi*D=50','r=5; D=2; q/4*Pi*D=100');

%Clear all values
clear all;

%Initialize counter
n=1;

%Set time vector
t=linspace(0.01,5,1000);

%Set parameters
a=25;
r=1.25;
D=2;

while n < 1001
    c(n)=(a/r)*erfc(r/(2*(D*t(n))^(1/2)));
    n=n+1;
end

%Reset counter
n=1;
```

```
%Re-set parameters
a=25;
r=1.875;
D=2;

while n < 1001
    c2(n)=(a/r)*erfc(r/(2*(D*t(n))^(1/2)));
    n=n+1;
end

%Reset counter
n=1;

%Re-set parameters
a=25;
r=2.5;
D=2;

while n < 1001
    c3(n)=(a/r)*erfc(r/(2*(D*t(n))^(1/2)));
    n=n+1;
end

%Reset counter
n=1;

%Re-set parameters
a=25;
r=5;
D=2;

while n < 1001
    c4(n)=(a/r)*erfc(r/(2*(D*t(n))^(1/2)));
    n=n+1;
end

%Reset counter
n=1;

%Re-set parameters
a=25;
r=20;
D=2;

while n < 1001
    c5(n)=(a/r)*erfc(r/(2*(D*t(n))^(1/2)));
    n=n+1;
end

%Plot figure
figure(2)
plot(t,c,'-.',t,c2,'-.',t,c3,'-.',t,c4,'-.',t,c5,'-.');
title('Early post-administration tissue distribution of liposomes');
```

```
xlabel('Time, t');
ylabel('Concentration, C');
legend('r=1.25; D=2; q/4*Pi*D=25','r=1.875; D=2; q/4*Pi*D=25','r=2.5;
D=2; q/4*Pi*D=25','r=5; D=2; q/4*Pi*D=25','r=20; D=2; q/4*Pi*D=25');

%Clear all values
clear all;

%Initialize counter
n=1;

%Set position vector
r=linspace(1,5,1000);

%Set parameters
a=6.25;
t=5;
D=2;

while n < 1001
    c(n)=(a/r(n))*erfc(r(n)/(2*(D*t)^(1/2)));
    n=n+1;
end

%Reset counter
n=1;

%Re-set parameters
a=6.25;
t=50;
D=2;

while n < 1001
    c2(n)=(a/r(n))*erfc(r(n)/(2*(D*t)^(1/2)));
    n=n+1;
end

%Reset counter
n=1;

%Re-set parameters
a=6.25;
t=500;
D=2;

while n < 1001
    c3(n)=(a/r(n))*erfc(r(n)/(2*(D*t)^(1/2)));
    n=n+1;
end

%Reset counter
n=1;

%Re-set parameters
```

```
a=6.25;
t=5000;
D=2;

while n < 1001
    c4(n)=(a/r(n))*erfc(r(n)/(2*(D*t)^(1/2)));
    n=n+1;
end

%Reset counter
n=1;

%Re-set parameters
a=6.25;
t=50000;
D=2;

while n < 1001
    c5(n)=(a/r(n))*erfc(r(n)/(2*(D*t)^(1/2)));
    n=n+1;
end

%Plot figure
figure(3)
plot(r,c,'-.',r,c2,'-.',r,c3,'-.',r,c4,'-.',r,c5,'-.');
title('Early post-administration tissue distribution of liposomes');
xlabel('Position, r');
ylabel('Concentration, C');
legend('t=5; D=2; q/4*Pi*D=6.25','t=50; D=2; q/4*Pi*D=6.25','t=500;
D=2; q/4*Pi*D=6.25','t=5000; D=2; q/4*Pi*D=6.25','t=50000; D=2;
q/4*Pi*D=6.25');

%Clear all at the end of the program
clear all;


function Model_IV
clear all;
close all;

%Input experimental data
C=[42 31 21 15 9 4.1 2.8 1.9 0.99];
t=[0.25 0.5 1 1.5 2 4 8 12 16];

[alpha,R,J]=nlinfit(t,C,@fit,[1 1 1 1]);

alpha

%Plot nonlinear regression fit
figure(1),clf,
semilogy(t,C,'.');
hold on;
semilogy(t,alpha(1)*exp(-alpha(2)*t)+alpha(3)*exp(-alpha(4)*t),'-.');
title('Liposome clearance from blood');
xlabel('Time, t');
```

```
ylabel('Concentration, C');
legend('C_p=47.2e^-^1^.^1^t+5.6e^-^0^.^1^t');
hold off;

%Clear all at the end of the program
clear all;

function alwong_Model_IV = fit(alpha,t)
alwong_Model_IV=alpha(1)*exp(-alpha(2)*t)+alpha(3)*exp(-alpha(4)*t);


function Model_V
clc;
clear all;
close all;

%Set parameters
d=0.02;
L=0.1E-5;
u=2.5;
k=0.2;

%Set initial conditions
ICs=[500; 50000; 0];

%Set length to solve the system
z=linspace(0,L,20000);

%Set numerical solver options
options=odeset('NonNegative',[1 2 3]);

[length C]=ode15s(@equations,z,ICs,options,d,u,k);

%Plot liquid-phase concentrations as function of PFR position
figure(1)
plot(length,C(:,1),'-.',length,C(:,2),'-.');
title('Drug-encapsulating liposome (DEL) production in a PFR');
xlabel('PFR Position, L');
ylabel('Solution-Phase Concentration, C');
legend('[MER]','[DRG]');
axis([0 0.1E-6 0 5E4]);

figure(2)
plot(length,C(:,1),'-.');
title('Drug-encapsulating liposome (DEL) production in a PFR');
xlabel('PFR Position, L');
ylabel('Solution-Phase Concentration, C');
legend('[MER]');
axis([0 0.1E-6 0 500]);

figure(3)
plot(length,C(:,3),'-.');
title('Drug-encapsulating liposome (DEL) production in a PFR');
xlabel('PFR Position, L');
ylabel('Solution-Phase Concentration, C');
```

```
legend('[DEL]');
axis([0 0.1E-6 0 10]);

%Clear all at the end of the program
clear all;

function alwong_Model_V = equations(L,C,d,u,k)
dCdt=zeros(3,1);
Mer=C(1);
Drg=C(2);
Del=C(3);

dCdt(1)=-(400/d)*k*Mer*Drg;
dCdt(2)=-(40000/d)*k*Mer*Drg;
dCdt(3)=(4/d)*k*Mer*Drg;

alwong_Model_V=(1/u)*dCdt;
return;
```

Appendix B

Mathematical Models Supplement

B.a Simplified Drug Leakage from Multilamellar Liposome Vesicles (MLVs)

This section presents a simplified version of Mathematical Model I in the limiting case where any drug reaching the external surface of the MLV is almost instantaneously convected away due to a high rate of convection in the fluid outside the MLV (i.e., $C \approx 0$ at $r = R$).

The governing PDE in this case, with IC and BCs, is:

$$\frac{\partial C}{\partial t} = D\left[\frac{1}{r^2}\frac{\partial}{\partial r}\left(r^2\frac{\partial C}{\partial r}\right)\right] \tag{a.1}$$

$$0 < r < R \quad t \le 0 \qquad C = C_0 \tag{a.2}$$

$$r = 0 \quad t \ge 0 \qquad \frac{\partial C}{\partial r} = 0 \tag{a.3}$$

$$r = R \quad t \ge 0 \qquad C = 0 \tag{a.4}$$

Scaling and nondimensionalizing, we obtain:

$$\eta = \frac{r}{R} \qquad \theta' = \frac{C}{C_0} \qquad \tau = \frac{D}{R^2}t \tag{a.5}$$

$$\frac{\partial \theta'}{\partial \tau} = \frac{1}{\eta^2}\frac{\partial}{\partial \eta}\left(\eta^2\frac{\partial \theta'}{\partial \eta}\right) \tag{a.6}$$

$$0 < \eta < 1 \quad \tau \le 0 \qquad \theta' = 1 \tag{a.7}$$

$$\eta = 0 \quad \tau \ge 0 \qquad \frac{\partial \theta'}{\partial \eta} = 0 \tag{a.8}$$

$$\eta = 1 \quad \tau \ge 0 \qquad \theta' = 0 \tag{a.9}$$

We now apply the transformation:

$$\theta(\eta,\tau) = 1 - \theta'(\eta,\tau) \tag{a.10}$$

Then:

$$\frac{\partial\theta}{\partial\tau} = \frac{1}{\eta^2}\frac{\partial}{\partial\eta}\left(\eta^2\frac{\partial\theta}{\partial\eta}\right) \tag{a.11}$$

$$0 < \eta < 1 \quad \tau \le 0 \qquad \theta = 0 \tag{a.12}$$

$$\eta = 0 \quad \tau \ge 0 \qquad \frac{\partial\theta}{\partial\eta} = 0 \tag{a.13}$$

$$\eta = 1 \quad \tau \ge 0 \qquad \theta = 1 \tag{a.14}$$

Using the finite Fourier transform (FFT) method, we seek a solution of the form:

$$\theta(\eta,\tau) = \sum_{n=1}^{\infty}\theta_n(\tau)\phi_n(\eta) \tag{a.15}$$

Per Deen [29], the basis functions required are those satisfying Dirichlet boundary conditions, specifically:

$$\phi_n(\eta) = \sqrt{2}\,\frac{\sin(n\pi\eta)}{\eta}\ , \qquad n = 1, 2, \ldots \tag{a.16}$$

Transforming the time and space derivatives in Eq. a.11, we obtain:

$$\int_0^1 \phi_n\frac{\partial\theta}{\partial\tau}\eta^2 d\eta = \frac{d\theta_n}{d\tau} \tag{a.17}$$

$$\int_0^1 \phi_n\left[\frac{1}{\eta^2}\frac{\partial}{\partial\eta}\left(\eta^2\frac{\partial\theta}{\partial\eta}\right)\right]\eta^2 d\eta = \eta^2\left(\phi_n\frac{\partial\theta}{\partial\eta} - \theta\frac{d\phi_n}{d\eta}\right)_{\eta=0}^{\eta=1} - \lambda_n^2\theta_n = -\sqrt{2}(n\pi)(-1)^n - (n\pi)^2\theta_n \tag{a.18}$$

The initial condition transforms simply to:

$$\theta_n(0) = 0 \tag{a.19}$$

Accordingly, the complete transformed problem is:

$$\frac{d\theta_n}{d\tau} + (n\pi)^2\theta_n = -\sqrt{2}(n\pi)(-1)^n\ , \qquad \theta_n(0) = 0 \tag{a.20}$$

The solution of Eq. a.20 is:

$$\theta_n = -\left[\frac{\sqrt{2}(-1)^n}{n\pi}\right]\left\{1-\exp\left[-(n\pi)^2\tau\right]\right\} \tag{a.21}$$

The overall solution, then, using Eq. a.16 and a.21 in Eq. a.15, is:

$$\theta(\eta,\tau) = \sum_{n=1}^{\infty}\left[\frac{-2(-1)^n}{n\pi\eta}\right]\sin(n\pi\eta)\left\{1-\exp\left[-(n\pi)^2\tau\right]\right\} \tag{a.22}$$

Following the analysis of Deen [29], inspection shows that the solution in Eq. a.22 consists of two main parts: a transient part which decays exponentially over time and a time-independent part which represents a steady state achieved as $\tau \rightarrow \infty$. Eq. a.22 is hence rewritten more simply using the steady-state solution as:

$$\theta(\eta,\tau) = 1 + \sum_{n=1}^{\infty}\left[\frac{2(-1)^n}{n\pi\eta}\right]\sin(n\pi\eta)\exp\left(-n^2\pi^2\tau\right) \tag{a.23}$$

Finally, using Eq. a.23 in Eq. a.10, we obtain:

$$\theta'(\eta,\tau) = \sum_{n=1}^{\infty}\left[\frac{-2(-1)^n}{n\pi\eta}\right]\sin(n\pi\eta)\exp\left(-n^2\pi^2\tau\right) \tag{a.24}$$

$$\eta = \frac{r}{R} \qquad \theta' = \frac{C}{C_0} \qquad \tau = \frac{D}{R^2}t \tag{a.5}$$

Eq. a.24, in conjunction with Eq. a.5, provides a representation of the concentration C of a given drug in a spherically symmetric, homogeneous drug-encapsulating MLV of radius R as a function of radial position and time. Eq. a.24 hence, given three basic parameters: the initial (post-loading) concentration C_0 of the drug in question in the MLV in question, the diffusivity D of said drug in said MLV, and the radius R of said MLV, allows one to easily quantitatively model and predict drug leakage over time from drug-encapsulating MLVs for many drug and homogeneous MLV combinations.

The following MATLAB code can be used (with slight modifications as necessary) to numerically evaluate and graphically portray the dimensionless concentration θ' of a given drug in a spherically symmetric, homogeneous drug-encapsulating MLV of radius R as a function of dimensionless radial position η and dimensionless time τ:

```
function Model_B_I
clear all;
close all;

%Initialize counter
c=1;

%Set initial dimensionless position
r=0.001;

n=1:100;

while r < 1.001
    a=(((-2)*(-1).^n)./(r*n*pi)).*sin(r*n*pi).*exp(-(n.^2)*pi*pi*.005);
    temp=cumsum(a);
    s(c)=temp(1,100);
    rv(c)=r;
    r=r+0.001;
    c=c+1;
end

%Reset counter for next 'tau' value
c=1;

%Set initial dimensionless position
r=0.001;

while r < 1.001
    a=(((-2)*(-1).^n)./(r*n*pi)).*sin(r*n*pi).*exp(-(n.^2)*pi*pi*.01);
    temp=cumsum(a);
    sa(c)=temp(1,100);
    rv(c)=r;
    r=r+0.001;
    c=c+1;
end

%Reset counter for next 'tau' value
c=1;

%Set initial dimensionless position
r=0.001;

while r < 1.001
    a=(((-2)*(-1).^n)./(r*n*pi)).*sin(r*n*pi).*exp(-(n.^2)*pi*pi*.05);
```

```
    temp=cumsum(a);
    sb(c)=temp(1,100);
    rv(c)=r;
    r=r+0.001;
    c=c+1;
end

%Reset counter for next 'tau' value
c=1;

%Set initial dimensionless position
r=0.001;

while r < 1.001
    a=(((-2)*(-1).^n)./(r*n*pi)).*sin(r*n*pi).*exp(-(n.^2)*pi*pi*.1);
    temp=cumsum(a);
    sc(c)=temp(1,100);
    rv(c)=r;
    r=r+0.001;
    c=c+1;
end

%Reset counter for next 'tau' value
c=1;

%Set initial dimensionless position
r=0.001;

while r < 1.001
    a=(((-2)*(-1).^n)./(r*n*pi)).*sin(r*n*pi).*exp(-(n.^2)*pi*pi*.15);
    temp=cumsum(a);
    sd(c)=temp(1,100);
    rv(c)=r;
    r=r+0.001;
    c=c+1;
end

%Reset counter for next 'tau' value
c=1;

%Set initial dimensionless position
r=0.001;

while r < 1.001
    a=(((-2)*(-1).^n)./(r*n*pi)).*sin(r*n*pi).*exp(-(n.^2)*pi*pi*.2);
    temp=cumsum(a);
    se(c)=temp(1,100);
    rv(c)=r;
    r=r+0.001;
    c=c+1;
end

%Reset counter for next 'tau' value
c=1;
```

```
%Set initial dimensionless position
r=0.001;

while r < 1.001
    a=(((-2)*(-1).^n)./(r*n*pi)).*sin(r*n*pi).*exp(-(n.^2)*pi*pi*.3);
    temp=cumsum(a);
    sf(c)=temp(1,100);
    rv(c)=r;
    r=r+0.001;
    c=c+1;
end

%Reset counter for next 'tau' value
c=1;

%Set initial dimensionless position
r=0.001;

while r < 1.001
    a=(((-2)*(-1).^n)./(r*n*pi)).*sin(r*n*pi).*exp(-(n.^2)*pi*pi*.4);
    temp=cumsum(a);
    sg(c)=temp(1,100);
    rv(c)=r;
    r=r+0.001;
    c=c+1;
end

%Plot figure
figure(1)
plot(rv,s,'-.',rv,sa,'-.',rv,sb,'-.',rv,sc,'-.',rv,sd,'-.',rv,se,'-
.',rv, ...
    sf,'-.',rv,sg,'k-.');
title('Drug leakage from a drug-encapsulating MLV of radius R');
xlabel('Dimensionless Radial Position, r/R');
ylabel('Dimensionless Concentration, C/C_0');
legend('Dt/R^2 =
0.005','0.01','0.05','0.10','0.15','0.20','0.30','0.40');
axis([0.01 .99 -0.01 .99]);

%Clear all values
clear all;

%Initialize counter
c=1;

%Set initial dimensionless time
t=0.001;

n=1:100;

while t < 1.001
    a=(((-2)*(-1).^n)./(.005*n*pi)).*sin(.005*n*pi).*exp(-
(n.^2)*pi*pi*t);
    temp=cumsum(a);
    s(c)=temp(1,100);
```

```
    tv(c)=t;
    t=t+0.001;
    c=c+1;
end

%Reset counter for next 'eta' value
c=1;

%Set initial dimensionless time
t=0.001;

while t < 1.001
    a=(((-2)*(-1).^n)./(.25*n*pi)).*sin(.25*n*pi).*exp(-
(n.^2)*pi*pi*t);
    temp=cumsum(a);
    sa(c)=temp(1,100);
    tv(c)=t;
    t=t+0.001;
    c=c+1;
end

%Reset counter for next 'eta' value
c=1;

%Set initial dimensionless time
t=0.001;

while t < 1.001
    a=(((-2)*(-1).^n)./(.5*n*pi)).*sin(.5*n*pi).*exp(-(n.^2)*pi*pi*t);
    temp=cumsum(a);
    sb(c)=temp(1,100);
    tv(c)=t;
    t=t+0.001;
    c=c+1;
end

%Reset counter for next 'eta' value
c=1;

%Set initial dimensionless time
t=0.001;

while t < 1.001
    a=(((-2)*(-1).^n)./(.75*n*pi)).*sin(.75*n*pi).*exp(-
(n.^2)*pi*pi*t);
    temp=cumsum(a);
    sc(c)=temp(1,100);
    tv(c)=t;
    t=t+0.001;
    c=c+1;
end

%Reset counter for next 'eta' value
c=1;
```

```
%Set initial dimensionless time
t=0.001;

while t < 1.001
    a=(((-2)*(-1).^n)./(.95*n*pi)).*sin(.95*n*pi).*exp(-
(n.^2)*pi*pi*t);
    temp=cumsum(a);
    sd(c)=temp(1,100);
    tv(c)=t;
    t=t+0.001;
    c=c+1;
end

%Reset counter for next 'eta' value
c=1;

%Set initial dimensionless position
t=0.001;

while t < 1.001
    a=(((-2)*(-1).^n)./(.99*n*pi)).*sin(.99*n*pi).*exp(-
(n.^2)*pi*pi*t);
    temp=cumsum(a);
    se(c)=temp(1,100);
    tv(c)=t;
    t=t+0.001;
    c=c+1;
end

%Plot figure
figure(2)
plot(tv,s,'-.',tv,sa,'-.',tv,sb,'-.',tv,sc,'-.',tv,sd,'-.',tv,se,'-.');
title('Drug leakage from a drug-encapsulating MLV of radius R');
xlabel('Dimensionless Time, Dt/R^2');
ylabel('Dimensionless Concentration, C/C_0');
legend('r/R = 0.005','0.25','0.50','0.75','0.95','0.99');
axis([0 .99 -0.01 1.01]);

%Clear all at the end of the program
clear all;
```

Code Block B.a – MATLAB code for numerically evaluating and graphically portraying Eq. a.24.

A plot of the dimensionless concentration θ' of a given drug in a MLV as a function of dimensionless radial position η at various values of dimensionless time τ is shown in Figure 19, below:

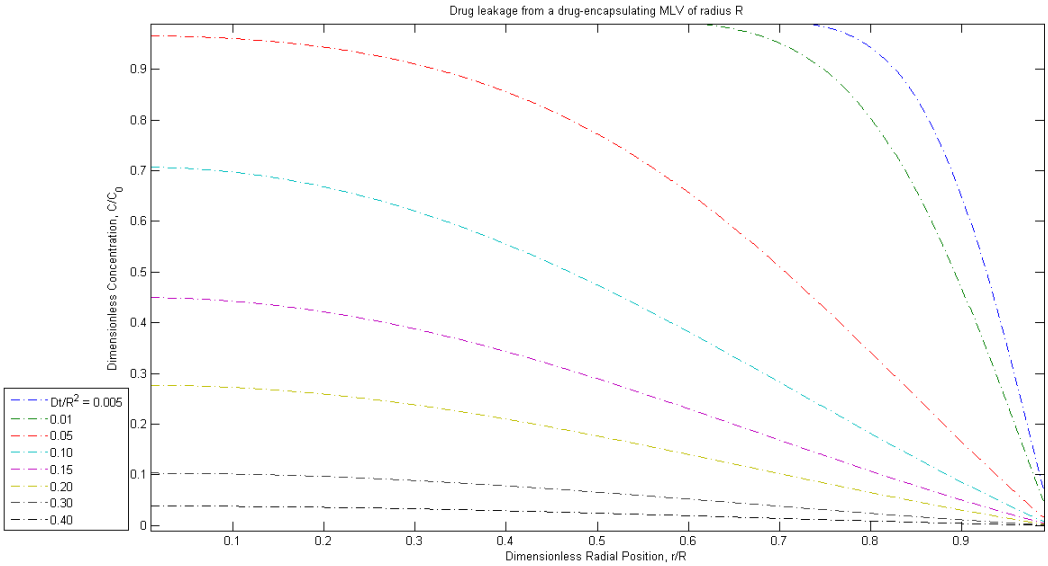

Figure 19 – Drug leakage from a drug-encapsulating MLV of radius *R*. The dimensionless drug concentration is shown as a function of dimensionless radial position at various values of dimensionless time.

A plot of the dimensionless concentration θ' of a given drug in a MLV as a function of dimensionless time τ at various values of dimensionless radial position η is shown in Figure 20, below:

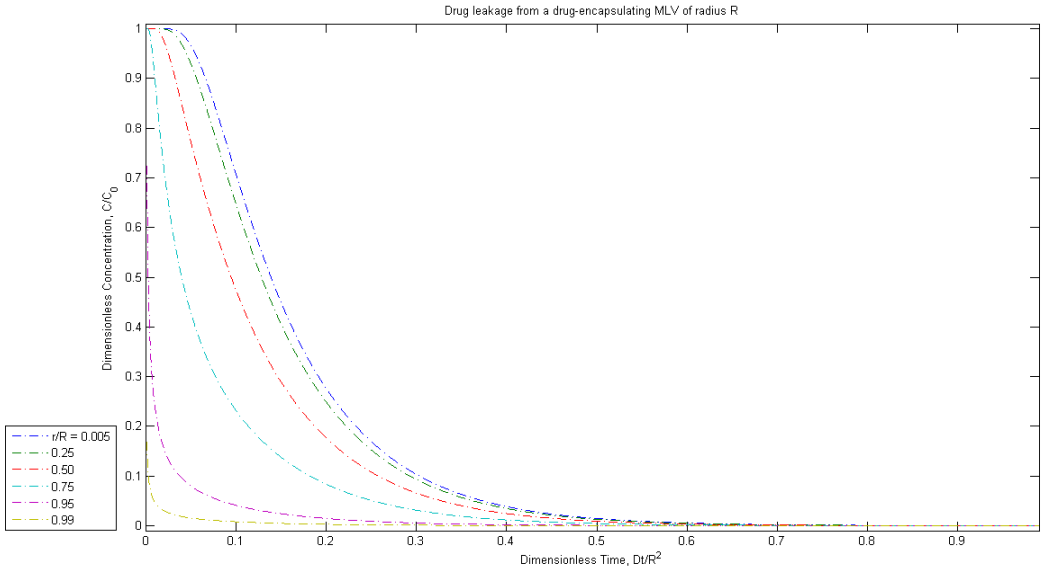

Figure 20 – Drug leakage from a drug-encapsulating MLV of radius *R*. The dimensionless drug concentration is shown as a function of dimensionless time at various values of dimensionless radial position.

Broadly, the plots shown in Figures 19 and 20, above, are consistent with qualitative expectations. At a given radial position, the concentration decays with scaled time. At a given scaled time point, the concentration decreases with increasing radial distance from the center of the drug-encapsulating MLV. Also, since the results and trends shown in Figures 10 and 11, above, involve dimensionless (normalized/scaled) quantities, they – and the results and trends one could obtain from similar plots – are applicable to any drug-encapsulating MLV system that Eq. a.24 is applicable to.

Model B.a Assumptions: spherically symmetric, homogeneous MLV; uniformly drug-saturated MLV; Fick's law valid; drug bulk concentration in the blood $C_{bulk,\ blood} = 0$ *compared to drug concentration in the liposome* $C_{liposome}$*; high rate of convection in fluid outside MLV (hence* $C \approx 0$ *at* $r = R$*); constant parameters (D, R, ρ); no reactions*

B.b Vascular Distribution of Liposomes

This section extends Mathematical Model II by using first principles to compute the mass transfer coefficient k_c and model the liposome distribution in a blood vessel in the limiting case where any drug reaching the inner vessel wall surface is almost instantaneously leaked into the tissue space (i.e., $C \approx 0$ at $r = R$).

The governing PDE in this case, with BCs, is:

$$2U\left\{1-\left(\frac{r}{R}\right)^2\right\}\frac{\partial C}{\partial z} = D\left\{\frac{1}{r}\frac{\partial}{\partial r}\left(r\frac{\partial C}{\partial r}\right)\right\} \tag{b.1}$$

$$C(r,0) = C_0 \tag{b.2}$$

$$C(R,z) = 0 \tag{b.3}$$

$$\frac{\partial C}{\partial r}(0,z) = 0 \tag{b.4}$$

Scaling, we define the following dimensionless variables:

$$\eta = \frac{r}{R} \qquad \theta = \frac{C}{C_0} \qquad \zeta = \frac{z}{R * \mathrm{Pe}} \tag{b.5}$$

where:

$$\mathrm{Pe} = \frac{2UR}{D} \tag{b.6}$$

Nondimensionalizing Eq. b.1-b.4, then, we obtain:

$$\left(1-\eta^2\right)\frac{\partial \theta}{\partial \zeta} = \frac{1}{\eta}\frac{\partial}{\partial \eta}\left(\eta\frac{\partial \theta}{\partial \eta}\right) \tag{b.7}$$

$$\theta(\eta,0) = 1 \tag{b.8}$$

$$\theta(1,\zeta) = 0 \tag{b.9}$$

$$\frac{\partial \theta}{\partial \eta}(0,\zeta) = 0 \tag{b.10}$$

We first solve for the Sherwood number in the liposome concentration entrance region. Following the analysis of Deen [29], we define a new dimensionless variable:

$$\psi = 1 - \eta \tag{b.11}$$

Then Eq. b.7 becomes:

$$\left(2\psi - \psi^2\right)\frac{\partial\theta}{\partial\zeta} = \frac{\partial^2\theta}{\partial\psi^2} - \frac{1}{1-\psi}\frac{\partial\theta}{\partial\psi} \tag{b.12}$$

Performing an order-of-magnitude analysis on each term in Eq. b.12 per Deen [29] and retaining only the dominant terms, we obtain:

$$2\psi\frac{\partial\theta}{\partial\zeta} = \frac{\partial^2\theta}{\partial\psi^2} \tag{b.13}$$

with boundary conditions:

$$\theta(\psi,0) = 1 \tag{b.14}$$

$$\theta(0,\zeta) = 0 \tag{b.15}$$

$$\theta(\infty,\zeta) = 1 \tag{b.16}$$

Per Deen [29], we now apply the similarity method to solve this PDE. We assume that θ can be expressed as a function of an independent variable s:

$$s = \frac{\psi}{g(\zeta)} \tag{b.17}$$

In terms of the similarity variable, Eq. b.13 becomes [29]:

$$\frac{d^2\theta}{ds^2} + 2s^2\left(g^2g'\right)\frac{d\theta}{ds} = 0 \tag{b.18}$$

Now requiring:

$$g^2g' = \text{constant} \equiv \frac{3}{2} \tag{b.19}$$

and

$$g(0) = 0 \tag{b.20}$$

we obtain:

$$g(\zeta) = \left(\frac{9}{2}\zeta\right)^{1/3} \tag{b.21}$$

$$s = \left(\frac{2}{9}\right)^{1/3} \frac{\psi}{\zeta^{1/3}} \tag{b.22}$$

Eq. b.18 now becomes [29]:

$$\frac{d^2\theta}{ds^2} + 3s^2 \frac{d\theta}{ds} = 0 \tag{b.23}$$

with boundary conditions:

$$\theta(0) = 0 \tag{b.24}$$

$$\theta(\infty) = 1 \tag{b.25}$$

Solving Eq. b.23, then:

$$\theta(s) = 1 - \frac{3}{\Gamma(1/3)} \int_s^\infty e^{-t^3} dt \tag{b.26}$$

Per Deen [29], then, the Sherwood number can now be calculated as:

$$\text{Sh} \equiv \frac{2k_c R}{D} = \frac{2(-\partial\theta/\partial\psi)|_{\psi=0}}{\theta_w - \theta_b} = 2\left.\frac{\partial\theta}{\partial\psi}\right|_{\psi=0} = \frac{6}{\Gamma(1/3) g(\zeta)} \tag{b.27}$$

where $\theta_b = 1$ because the liposome concentration in most of the vessel remains at the inlet concentration of 1.

Hence, in the liposome concentration entrance region:

$$\text{Sh} = 1.357\left(\frac{R}{z}\right)^{1/3} \text{Pe}^{1/3} \tag{b.28}$$

We now solve for the Sherwood number in the liposome concentration fully developed region [29]. Again, the PDE of interest, slightly rearranged, with BCs is:

$$\frac{\partial\theta}{\partial\zeta} = \frac{1}{\eta(1-\eta^2)} \frac{\partial}{\partial\eta}\left(\eta \frac{\partial\theta}{\partial\eta}\right) \tag{b.29}$$

$$\theta(\eta, 0) = 1 \tag{b.8}$$

$$\theta(1,\zeta)=0 \tag{b.9}$$

$$\frac{\partial\theta}{\partial\eta}(0,\zeta)=0 \tag{b.10}$$

Using the finite Fourier transform (FFT) method, we seek a solution of the form:

$$\theta(\eta,\zeta)=\sum_{n=1}^{\infty}\theta_n(\zeta)\phi_n(\eta) \tag{b.30}$$

The basis functions required are, per Deen [29]:

$$\phi_n(\eta)=a_n G(\lambda_n\eta) \tag{b.31}$$

The complete transformed problem is then:

$$\frac{d\theta_n}{d\zeta}+\lambda_n^2\theta_n=0\ , \qquad \theta_n(0)=\langle 1,\phi_n\rangle=b_n \tag{b.32}$$

Solving, the overall solution is [29]:

$$\theta(\eta,\zeta)=\sum_{n=1}^{\infty}a_n b_n e^{-\lambda_n^2\zeta}G(\lambda_n\eta) \tag{b.33}$$

The Sherwood number can then be calculated as:

$$\mathrm{Sh}\equiv\frac{2k_c R}{D}=\frac{-2}{\theta_b}\frac{\partial\theta}{\partial\eta}\bigg|_{\eta=1} \tag{b.34}$$

Applying an overall species balance and integrating from ∞ to a finite value of ζ:

$$\theta_b(\zeta)=-4\int_{\zeta}^{\infty}\frac{\partial\theta}{\partial\eta}(1,v)dv \tag{b.35}$$

where *v* is a dummy variable. Then, for $\zeta\to\infty$:

$$\theta(\eta,\zeta)\to a_1 b_1 e^{-\lambda_1^2\zeta}G(\lambda_1\eta) \tag{b.36}$$

$$\frac{\partial\theta}{\partial\eta}(1,\zeta)\to a_1 b_1 e^{-\lambda_1^2\zeta}\lambda_1\frac{dG}{d\eta}(\lambda_1) \tag{b.37}$$

$$\theta_b(\zeta)=-4\frac{a_1 b_1}{\lambda_1}e^{-\lambda_1^2\zeta}\frac{dG}{d\eta}(\lambda_1) \tag{b.38}$$

Using Eq. b.37-b.38 in Eq. b.34, then, the fully developed Sherwood number is simply:

$$\mathrm{Sh}(\infty) = \frac{1}{2}\lambda_1^2 \tag{b.39}$$

which can be evaluated to yield:

$$\mathrm{Sh}(\infty) = 3.657 \tag{b.40}$$

The equations above provide a representation of the distribution of (drug-encapsulating or non-drug-encapsulating) liposomes in a blood vessel as a function of radial and axial position. The model hence, given three basic parameters: the radius R of the vessel, the mean velocity U of fluid flow in said vessel, and the diffusivity D of the liposomes in said vessel, allows one to compute the mass transfer coefficient k_c and quantitatively model and predict the spatial distribution of liposomes in a blood vessel for many types of liposomes. The model can be refined by taking into account certain processes, shown in Figure 21, below, neglected in the above analysis for the sake of obtaining an analytical solution.

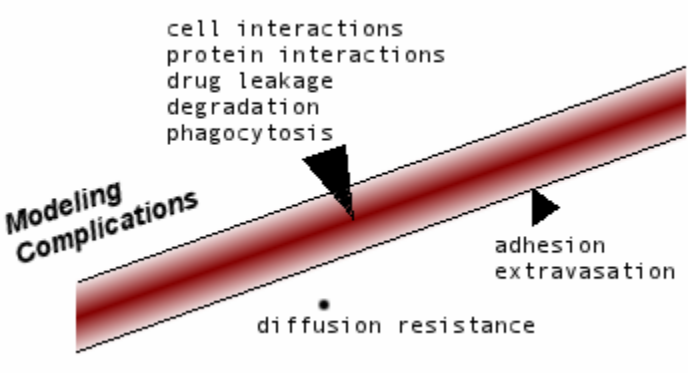

Figure 21 – Schematic showing complicating factors potentially having an impact on the vascular distribution of liposomes.

*Model B.b Assumptions: incompressible Newtonian blood; Fick's law valid; fully developed blood flow; unidirectional, axisymmetric blood flow; steady blood flow; large Péclet number (Pe = 2*U*R/D ~ 2*(0.001 m/s)*(5*10^{-6} m)/(10^{-12} m^2/s) = 10^4 >> 1 in a*

capillary); $d\mathcal{P}/dz$ = constant; high rate of diffusion of liposomes through vessel wall (hence $C \approx 0$ at $r = R$); constant parameters (D, R, μ, ρ); no reactions

References and Further Reading

1. **Kumar, V., N. Fausto, and A. Abbas.** 2004. Robbins and Cotran pathologic basis of disease. Saunders, St. Louis, MO.
2. **Gansauge, F., S. Gansauge, E. Schmidt, J. Muller, and H. G. Beger.** 1998. Prognostic significance of molecular alterations in human pancreatic carcinoma - an immunohistological study. Langenbeck's Arch. Sur. **383:**152-155.
3. **Poch, B., F. Gansauge, A. Schwarz, T. Seufferlein, T. Schnelldorfer, M. Ramadani, H. G. Beger, and S. Gansauge.** 2001. Epidermal growth factor induces cyclin D1 in human pancreatic carcinoma: evidence for a cyclin D1-dependent cell cycle progression. Pancreas **23:**280-287.
4. **Arnum, P. V.** 2006. Cytotoxic drug market will influence growth of high-potency active ingredients. Pharm. Tech. EPT
5. **DeAngelis, L. M., W. Seiferheld, S. C. Schold, B. Fisher, and C. J. Schultz.** 2002. Combination chemotherapy and radiotherapy for primary central nervous system lymphoma: radiation therapy oncology group study 93-10. J. Clin. Oncol. **20:**4643-4648.
6. **Forastiere, A. A., H. Goepfert, M. Maor, T. F. Pajak, R. Weber, W. Morrison, B. Glisson, A. Trotti, J. A. Ridge, C. Chao, G. Peters, D. Lee, A. Leaf, J. Ensley, and J. Cooper.** 2003. Concurrent chemotherapy and radiotherapy for organ preservation in advanced laryngeal cancer. N. Engl. J. Med. **349:**2091-2098.
7. **Robert, C., J. C. Soria, and O. Chosidow.** 2006. Folliculitis and perionyxis associated with the EGFR inhibitor erlotinib. Targeted Oncol. **1:**100-103.
8. **Agero, A. L. C., S. W. Dusza, C. Benvenuto-Andrade, K. J. Busam, P. Myskowski, and A. C. Halpern.** 2006. Dermatologic side effects associated with the epidermal growth factor receptor inhibitors. J. Am. Acad. Dermatol. **55:**657-670.
9. **Galimont-Collen, A. F. S., L. E. Vos, A. P. M. Lavrijsen, J. Ouwerkerk, and H. Gelderblom.** 2007. Classification and management of skin, hair, nail and

mucosal side-effects of epidermal growth factor receptor (EGFR) inhibitors. Eur. J. Cancer **43:**845-851.

10. **Mouritsen, O. G.** 2005. Life-as a matter of fat: the emerging science of lipidomics. Springer, Berlin, De.
11. **Gerasimov, O. V., J. A. Boomer, M. M. Qualls, and D. H. Thompson.** 1999. Cytosolic drug delivery using pH- and light-sensitive liposomes. Adv. Drug Del. Rev. **38:**317-338.
12. **Dromi, S., V. Frenkel, A. Luk, B. Traughber, M. Angstadt, M. Bur, J. Poff, J. Xie, S. K. Libutti, K. C. P. Li, and B. J. Wood.** 2007. Pulsed-high intensity focused ultrasound and low temperature-sensitive liposomes for enhanced targeted drug delivery and antitumor effect. Clin. Cancer Res. **13:**2722-2727.
13. **DeSilva, N. S.** 2003. Interactions of surfactant protein D with fatty acids. Am. J. Respir. Cell Mol. Biol. **29:**757-770.
14. **Grabarek, Z. and J. Gergely.** 1990. Zero-length crosslinking procedure with the use of active esters. Anal. Biochem. **185:**131-135.
15. **Panayotou, G. N., A. I. Magee, and M. J. Geisow.** 1985. Reconstitution of the epidermal growth factor receptor in artificial lipid bilayers. FEBS Lett. **183:**321-325.
16. **Mimms, L. T., G. Zampighi, Y. Nozaki, C. Tanford, and J. A. Reynolds.** 1981. Phospholipid vesicle formation and transmembrane protein incorporation using octyl glucoside. Biochemistry **20:**833-840.
17. **Ge, G., J. Wu, and Q. Lin.** 2001. Effect of membrane fluidity on tyrosine kinase activity of reconstituted epidermal growth factor receptor. Biochem. Biophys. Res. Commun. **282:**511-514.
18. **Tuthill, T. J., D. Bubeck, D. J. Rowlands, and J. M. Hogle.** 2006. Characterization of early steps in the poliovirus infection process: receptor-decorated liposomes induce conversion of the virus to membrane-anchored entry-intermediate particles. J. Virol. **80:**172-180.
19. **Schneider, W. J.** 1983. Reconstitution of the low density lipoprotein receptor. J. Cell. Biochem. **23:**95-106.

20. **Lemmon, M. A., Z. Bu, J. E. Ladbury, M. Zhou, D. Pinchasi, I. Lax, D. M. Engelman, and J. Schlessinger.** 1997. Two EGF molecules contribute additively to stabilization of the EGFR dimer. EMBO J. **16:**281-294.
21. **Schlessinger, J.** 2002. Ligand-induced, receptor-mediated dimerization and activation of EGF receptor. Cell **110:**669-672.
22. **Lax, I., A. K. Mitra, C. Ravera, D. R. Hurwitz, M. Rubinstein, A. Ullrich, R. M. Stroud, and J. Schlessinger.** 1991. Epidermal growth factor (EGF) induces oligomerization of soluble, extracellular, ligand-binding domain of EGF receptor. J. Biol. Chem. **266:**13828-13833.
23. **Maurer, N., K. F. Wong, M. J. Hope, and P. R. Cullis.** 1998. Anomalous solubility behavior of the antibiotic ciprofloxacin encapsulated in liposomes: a ^{1}H-NMR study. Biochim. Biophys. Acta **1374:**9-20.
24. **Juretschke, H. P. and A. Lapidot.** 1984. Actinomycin D, ^{1}H NMR studies on intramolecular interactions and on the planarity of the chromophore. Eur. J. Biochem. **143:**651-658.
25. **Wittung, P., J. Kajanus, M. Kubista, and B. G. Malmstrom.** 1994. Absorption flattening in the optical spectra of liposome-entrapped substances. FEBS Lett. **352:**37-40.
26. **Hilmer, S. N., V. C. Cogger, M. Muller, and D. G. Le Conteur.** 2004. The hepatic pharmacokinetics of doxorubicin and liposomal doxorubicin. Drug Metab. Disp. **32:**794-799.
27. **Feigenson, G. W.** 1974. Nuclear magnetic relaxation studies of lecithin bilayers. California Institute of Technology, Pasadena, CA.
28. **Egelhaaf, S. U., E. Wehrli, M. Muller, M. Adrian, and P. Schurtenberger.** 1996. Determination of the size distribution of lecithin liposomes: a comparative study using freeze fracture, cryoelectron microscopy and dynamic light scattering. J. Micros. **184:**214-228.
29. **Deen, W. M.** 1998. Analysis of Transport Phenomena. Oxford University Press, New York, NY.

30. **Balakrishnan, B., J. F. Dooley, G. Kopia, and E. R. Edelman.** 2007. Intravascular drug release kinetics dictate arterial drug deposition, retention, and distribution. J. Cont. Rel. **123:**100-108.
31. **Shargel, L. and A. B. C. Yu.** 1993. Applied Biopharmaceutics and Pharmacokinetics. Appleton & Lange, Norwalk, CT.
32. **Northfelt, D. W., F. J. Martin, P. Working, P. A. Volberding, J. Russell, M. Newman, M. A. Amantea, and L. D. Kaplan.** 1996. Doxorubicin encapsulated in liposomes containing surface-bound polyethylene glycol: pharmacokinetics, tumor localization, and safety in patients with AIDS-related Kaposi's sarcoma. J. Clin. Pharmacol. **36:**55-63.
33. **Rahman, A., J. Treat, J. Roh, L. A. Potkul, W. G. Alvord, D. Forst, and P. V. Woolley.** 1990. A Phase I clinical trial and pharmacokinetic evaluation of liposome-encapsulated doxorubicin. J. Clin. Oncol. **8:**1093-1100.
34. **Marier, J., J. Lavigne, and M. P. Ducharme.** 2002. Pharmacokinetics and efficacies of liposomal and conventional formulations of tobramycin after intratracheal administration in rats with pulmonary *Burkholderia cepacia* infection. Antimicrob. Agents Chemother. **46:**3776-3781.
35. **Carneiro, A. L. and M. H. A. Santana.** 2004. Production of liposomes in a multitubular system useful for scaling up of processes. Progr. Colloid Polym. Sci. **128:**273-277.
36. **Kullberg, E. B., N. Bergstrand, J. Carlsson, K. Edwards, M. Johnsson, S. Sjberg, and L. Gedda.** 2002. Development of EGF-conjugated liposomes for targeted delivery of boronated DNA-binding agents. Bioconjugate Chem. **13:**737-743.
37. **Ishida, O., K. Maruyama, H. Tanahashi, M. Iwatsuru, K. Sasaki, M. Eriguchi, and H. Yanagie.** 2001. Liposomes bearing polyethyleneglycol-coupled transferrin with intracellular targeting property to the solid tumors *in vivo*. Pharm. Res. **18:**1042-1048.
38. **Suita, T., T. Kamidate, M. Yonaiyama, and H. Watanabe.** 1997. Characterization of horseradish peroxidase-encapsulated liposomes prepared by an extrusion technique. Anal. Sci. **13:**577-581.

39. **Fogler, H. S.** 2006. Elements of Chemical Reaction Engineering. Pearson Prentice Hall, Upper Saddle River, NJ.
40. **Johnston, M. J. W., S. C. Semple, S. K. Klimuk, K. Edwards, M. L. Eisenhardt, E. C. Leng, G. Karlsson, D. Yanko, and P. R. Cullis.** 2006. Therapeutically optimized rates of drug release can be achieved by varying the drug-to-lipid ratio in liposomal vincristine formulations. Biochim. Biophys. Acta **1758:**55-64.
41. **Majumdar, S., D. Flasher, D. S. Friend, P. Nassos, D. Yajko, W. K. Hadley, and N. Duzgunes.** 1992. Efficacies of liposome-encapsulated streptomycin and ciprofloxacin against *Mycobacterium avium-M. intracellulare* complex infections in human peripheral blood monocyte/macrophages. Antimicrob. Agents Chemother. **36:**2808-2815.
42. **Roessner, C. A. and G. M. Ihler.** 1984. Proteinase sensitivity of bacteriophage lambda tail proteins gpJ and pH in complexes with the lambda receptor. J. Bacteriol. **157:**165-170.
43. **Roessner, C. A., D. K. Struck, and G. M. Ihler.** 1983. Injection of DNA into liposomes by bacteriophage λ. J. Biol. Chem. **258:**643-648.
44. **Xu, Q., Y. Tanaka, and J. T. Czernuszka.** 2007. Encapsulation and release of a hydrophobic drug from hydroxyapatite coated liposomes. Biomaterials **28:**2687-2694.
45. **Roberts, M. J., M. D. Bentley, and J. M. Harris.** 2002. Chemistry for peptide and protein PEGylation. Adv. Drug Del. Rev. **54:**459-476.
46. **Tsai, W., A. D. Morielli, and E. G. Peralta.** 1997. The m1 muscarinic acetylcholine receptor transactivates the EGF receptor to modulate ion channel activity. EMBO J. **16:**4597-4605.
47. **Ross, S. M.** 1974. A mathematical model of mass transport in a long permeable tube with radial convection. J. Fluid Mech. **63:**157-175.
48. **Colton, C. K., K. A. Smith, P. Stroeve, and E. W. Merrill.** 1971. Laminar flow mass transfer in a flat duct with permeable walls. AIChE J. **17:**773-780.

Credits

1. http://www.anatomyacts.co.uk/learning/primary/Montage.htm
2. http://www.bioteach.ubc.ca/Bio-industry/Inex/
3. http://en.wikipedia.org/wiki/File:1NQL.png
4. http://en.wikipedia.org/wiki/File:4-Methylbenzoic_acid.png
5. http://en.wikipedia.org/wiki/File:Doxorubicin_chemical_structure.png
6. http://www.medscape.com/content/1999/00/41/79/417943/417943_fig.html
7. http://www.a-star.edu.sg/a_star/189-Press-Release?iid=238
8. Adobe Acrobat Professional. Adobe Systems Incorporated, San Jose, CA.
9. Cisco Systems VPN Client. Cisco Systems, Inc., San Jose, CA.
10. GIMP. The GIMP Development Team.
11. Mathematica. Wolfram Research, Champaign, IL.
12. MATLAB. The MathWorks, Natick, MA.
13. Microsoft Office Excel. Microsoft Corporation, Redmond, WA.
14. Microsoft Office Word. Microsoft Corporation, Redmond, WA.
15. ScienceDirect. Elsevier B.V., Amsterdam, Nl.
16. SciFinder Scholar. Chemical Abstracts Service, Columbus, OH.